REVIEW ARTICLE | JUNE 05 2023

DFT + μ: Density functional theory for muon site determination

S. J. Blundell ; T. Lancaster

Appl. Phys. Rev. 10, 021316 (2023)
https://doi.org/10.1063/5.0149080

Applied Physics Reviews REVIEW pubs.aip.org/aip/are

DFT + μ: Density functional theory for muon site determination

Cite as: Appl. Phys. Rev. **10**, 021316 (2023); doi: 10.1063/5.0149080
Submitted: 3 March 2023 · Accepted: 20 April 2023 ·
Published Online: 5 June 2023

S. J. Blundell[1,a] and T. Lancaster[2,a]

AFFILIATIONS

[1]Department of Physics, Clarendon Laboratory, Oxford University, Parks Road, Oxford OX1 3PU, United Kingdom
[2]Department of Physics, Centre for Materials Physics, Durham University, Durham DH1 3LE, United Kingdom

[a]Authors to whom correspondence should be addressed: stephen.blundell@physics.ox.ac.uk and tom.lancaster@durham.ac.uk

ABSTRACT

The technique of muon spin rotation (μSR) has emerged in the last few decades as one of the most powerful methods of obtaining local magnetic information. To make the technique fully quantitative, it is necessary to have an accurate estimate of where inside the crystal structure the muon implants. This can be provided by density functional theory calculations using an approach that is termed as DFT + μ, density functional theory with the implanted muon included. This article reviews this approach, describes some recent successes in particular μSR experiments, and suggests some avenues for future exploration.

TABLE OF CONTENTS

I. INTRODUCTION

Very often, in condensed matter physics, it is necessary to have very detailed information about the magnetic properties of materials measured at a local level. Standard magnetic characterization can be provided by measurements of magnetic susceptibility χ; this quantifies the magnetic response of a sample, revealed by its magnetic moment m induced by an applied field H, and ideally extracted in the limit of $H \to 0$, so that $\chi = \lim_{H\to 0} M/H$, where M is the magnetization $M = m/V$, and V is the sample's volume. This has two obvious problems: (1) the limit of $H \to 0$ is hard to achieve since the magnitude of the measurement signal is often proportional to H, so measurements have to be performed in non-zero, and sometimes substantial, applied field; (2) the measurement averages over the entire sample volume, since $m = \int_V M\,\mathrm{d}V$, and so there is no way to distinguish between a sample that is uniformly ordered, but with a small M, and one that is not ordered, but has a small component that is ordered with a large M. In such cases, what is needed is a highly sensitive local magnetic probe, ideally one operating at the atomic level and giving single spin detection.

Spin-polarized muons provide exactly this kind of sensitive local magnetic probe.[1–4] In a muon spin rotation (μSR) experiment, a beam of spin-polarized muons is implanted in the sample to be studied. When each muon decays, a positron and two neutrinos are emitted. A property of this decay is that the positron is not emitted isotropically, but preferentially along the direction of the muon spin at the moment of decay.[5] Detecting the direction along which the positron is emitted allows one to infer which direction the muon spin was pointing at the moment of its decay. Each muon lives for a different amount of time (according to the radioactive decay law) and so each muon decay gives rise to a positron whose detection at time t at a particular angle of emission contributes to a data point. Making many such positron

detections, taken over many million muon decays, allows one to build up a histogram $A(t)$, yielding the average muon spin polarization $P(t)$ of the large ensemble of muons as a function of time, allowing both static and dynamic local fields to be probed.

The technique has a number of key advantages. First of all, muon beams have 100% spin polarization (owing to parity violation in the weak interaction), in contrast to the very weak thermal polarizations obtained in nuclei in nuclear magnetic resonance (NMR) experiments. Second, muons have a larger gyromagnetic ratio than any nucleus in NMR, resulting in high sensitivity. It is very helpful that there is no restriction or necessity for specific nuclear isotopes, with muons usable for measurements in any material (in contrast to both NMR and neutron scattering). The ability to use an extended field range for measurements, from zero field (ZF) up to 10 T, and a wide range of temperatures (using dilution refrigerators, helium cryostats, or furnaces) means that μSR experiments are compatible with a very wide range of sample environment. Finally, the technique allows the user to study the time dependence of local magnetic fields, and the technique gives access to dynamical information with a very wide range of correlation times (10^{-10}–10^{-5} s) that fit neatly between a.c. susceptibility[6] on one hand and neutron scattering[7] on the other (the longest times are limited by the muon lifetime and the shortest times depend on the local field distribution[4]). Consequently, it has been widely used to study problems in magnetism,[2] superconductivity,[8] organic conductors,[9] and many other systems (for an up-to-date review of applications of μSR to a very wide range of topics, see Ref. 4) and has become a frequently deployed method alongside other experimental techniques, such as magnetic neutron diffraction.[7]

Despite many successes of the technique, there is a perceived drawback of the technique that arises from the lack of knowledge of the muon's stopping site in materials, raising the question of which magnetic fields are actually being probed. Consider the dipolar field $\boldsymbol{B}_{\mathrm{dip}}$ measured by the muon, resulting from the ordered magnetic moments in the sample. The α-component of the dipolar ($\alpha = x$, y or z) is given by

$$B^{\alpha}_{\mathrm{dip}} = \sum_{j} \sum_{\beta} D^{\alpha\beta}_{j} m^{\beta}_{j}, \tag{1}$$

where the first sum is taken over all the magnetic moments $\boldsymbol{m}_j$ within the Lorentz sphere (i.e., out to a large enough radius from the muon) and the dipolar tensor for the jth moment at position $\boldsymbol{r}_j$ is given by

$$D^{\alpha\beta}_{j} = \frac{\mu_0}{4\pi R^3_j}\left(\frac{3R^{\alpha}_{j}R^{\beta}_{j}}{R^2_j} - \delta^{\alpha\beta}\right), \tag{2}$$

where $\boldsymbol{R}_j = \boldsymbol{r}_j - \boldsymbol{r}_\mu$, and $\boldsymbol{r}_\mu$ is the muon position. These expressions are often used to model ordered magnetic arrangements, and this can be a very good test of the validity of a muon site, but notice that the expressions depend on the coordinates $\boldsymbol{R}_j$, which are measured with respect to the (unknown) muon position $\boldsymbol{r}_\mu$. There are other contributions to the field at the muon site in addition to $\boldsymbol{B}_{\mathrm{dip}}$ (such as the hyperfine field and, in the case of ferromagnets, the Lorentz and demagnetization fields[4]), but $\boldsymbol{B}_{\mathrm{dip}}$ is the most significant and illustrates the point that the field at the muon site is a function of the unknown quantity $\boldsymbol{r}_\mu$.

Even more serious is the unknown effect that the positively charged muon has on its local environment, raising the question of whether intrinsic behavior is being measured, or whether instead the experimental results are caused by the presence of the implanted muon itself. One can suspect that, if the final muon stopping state involves relatively little contact hyperfine coupling, the stopped muon will resemble something like a bare particle playing the role of an interstitial defect, albeit "dressed" by interactions with the electronic system. This might involve, for example, the muon acquiring a screening cloud of electronic charge in a metal, or acquiring a strain field in an insulator as it deforms atoms in its vicinity. Knowledge of the muon's stopping site in such cases would allow us insight into the local fields and interactions at a known position. If the muon instead forms a bound paramagnetic state such as muonium, or induces a large spin density at its position, knowledge of the muon site would, therefore, allow us to identify the electronic state that gives rise to the measured hyperfine coupling constants, and hence direct insight into the local electronic structure. To address this drawback of μSR, a density functional theory (DFT) *ab initio* approach has been developed to determine the muon site.[10–13] We call this approach DFT $+\mu$, density functional theory with an implanted muon, and this review will describe the method and demonstrate some of its recent successes.

II. THE SITE PROBLEM

The location of the muon site is determined by all the electrostatic interactions in the system, including the distortions produced in the material by the presence of the implanted muon, and interactions between all the particles in the system. This is a complicated problem, but it is pretty well described by non-relativistic quantum mechanics. The system comprising the stopped muon and its host material can, therefore, be described by the Schrödinger equation, and so a computation of the wavefunction of the system should, in principle, be possible. The system is, however, rather large, comprising the muon and the large number of electrons and nuclei in the sample. This is a many body problem and, therefore, extremely complex. Even if we restrict ourselves to focusing only on the electronic part of the wave function (which makes sense, as it is the behavior of the more mobile electrons that ultimately determines the muon site) the task is formidable.[14] In Sec. III, we will describe how this problem can be treated with electronic structure calculations, but in the remainder of this section, we will describe some methods that have been used previously.

A. The intuitive approach

Even without the use of sophisticated electronic structure calculations, it is possible to think about where a muon is likely to sit using chemical intuition. Most μSR experiments use positive muons (μ^+), and since the muon behaves like a light isotope of hydrogen, the μ^+ is likely to implant at a site that would be favored by the H^+ cation. Therefore, one can immediately deduce some *ad hoc* rules of thumb for guessing muon sites. For a start, one can conclude that positive muons favor sites close to negatively charged anions. A good example is provided by the large number of magnetic oxides that have been widely studied in condensed matter physics. In these, it is usually found that the muon sits around 1 Å from an O^{2-} ion (a result which was concluded during studies of the cuprate superconductors,[15] which all consist of a collection of cations and oxygen anions). The resulting state behaves like a hydroxyl OH group, which has a bond length close to 1 Å.[16] In fluorides, it is known that muons form F $-\mu-$ F bonds[17] in which the muon sits between the two fluoride ions, forming an

analogue of the bifluoride ion (HF_2^-). We will return to this important example later. In elemental metals, the muon would be expected to occupy a highly symmetrical site, such as an interstitial site inside the face-centred cubic lattice of copper for example.[18] These empirical rules of thumb are often useful and lead to the identification of highly plausible muon sites, albeit in a limited range of materials.

B. Bayesian methods

One fruitful approach to solving (or at least avoiding) the muon site problem is to deny that knowledge of the muon site is necessary. If the goal is to measure a magnetic moment of a magnetic ion in a structure, is the muon site really needed and can one include our quantified ignorance of it in the calculation? This approach leads to a Bayesian method[19] and is based on the observation that evaluating the dipolar field, given the muon site and the magnetic moment, is an easy problem [just use Eqs. (1) and (2)], but the reverse problem is hard. The inversion between the two calculations is accomplished using Bayes's theorem, which states that $P(\mathrm{A}|\mathrm{B}) = P(\mathrm{A})P(\mathrm{B}|\mathrm{A})/P(\mathrm{B})$. Here, $P(\mathrm{A})$ is called the *p*rior probability, since it is the probability of A occurring without any knowledge as to the outcome of B. The quantity which you derive is $P(\mathrm{A}|\mathrm{B})$, the *p*osterior probability. For the muon problem, we write Bayes's theorem as

$$P(\mu|\nu) = \frac{P(\mu)P(\nu|\mu)}{\int P(\nu|\mu')P(\mu')\,\mathrm{d}\mu'}, \tag{3}$$

where ν is a muon precession frequency, and μ is the magnetic moment of an ion in the crystal. Equation (3) gives the probability of a magnetic moment, given the observed muon precession frequency (the experimental problem, which is hard), in terms of the probability distribution of the muon precession frequency, given the size of the magnetic moment (the computational problem, which is easy). These are probabilities, since we do not know the muon site *a priori* and so the muon site is described by some probability distribution within the unit cell (and for the case of total ignorance of the muon site, the probability distribution can be uniform throughout the unit cell). Thus, we can compute the distribution of dipolar fields within the unit cell under some assumed distribution of muon sites (reflecting the level of our ignorance), which we can express as a probability density function (pdf) $f(\nu/\mu)$, evaluated as a function of precession frequency ν divided by magnetic moment μ (since the precession frequency scales with the magnetic moment). This function $f(\nu/\mu)$ allows us to evaluate $P(\nu|\mu)$ of Eq. (3). Thus, $P(\nu|\mu) = \frac{1}{\mu}f(\nu/\mu)$, and since $f(\nu/\mu)$ is normalized so that $\int f(\nu/\mu)\,\mathrm{d}(\nu/\mu) = 1$, the factor of $\frac{1}{\mu}$ is needed so that $\int P(\nu|\mu)\,\mathrm{d}\nu = 1$.

Since ν is obtained from a real experiment, what we would like to know is $g(\mu|\nu)$, the pdf of μ *given* the observed ν. This can be obtained from our calculated $f(\nu/\mu)$ using Bayes's theorem in the form of Eq. (3), which yields

$$g(\mu|\nu) = \frac{\frac{1}{\mu}f(\nu/\mu)}{\int_0^{\mu_{\max}} \frac{1}{\mu'}f(\nu/\mu')\,\mathrm{d}\mu'}, \tag{4}$$

where we have assumed a prior probability $[P(\mu)]$ for the magnetic moment that is uniform between zero and $\mu_{\max}$, and so, $P(\mu)$ is replaced by the uniform probability density $1/\mu_{\max}$ [which cancels on the top and bottom of Eq. (4)]. We choose $\mu_{\max}$ to take a large value, although it is found[19] that results are insensitive to the precise value of $\mu_{\max}$. When multiple frequencies ν_i are present in the spectra, it is necessary to multiply their probabilities of observation in order to obtain the chance of their simultaneous observation, so we evaluate $g(\mu|\{\nu_i\}) \propto \prod_i \int_{\nu_i-\Delta\nu_i}^{\nu_i+\Delta\nu_i} f(\nu_i/\mu)\,\mathrm{d}\nu_i$, where $\Delta\nu_i$ is the error on the fitted frequency. These results have been applied successfully in a number of studies.[19–22]

C. Knight shift measurements

An experimental method that has been used to identify or verify a muon site involves applying a transverse magnetic field $\boldsymbol{B}_{\mathrm{ext}}$ to the sample and measuring the Knight shift. This occurs because the field at the muon site $\boldsymbol{B}_\mu$ may not be exactly the same as the applied field $\boldsymbol{B}_{\mathrm{ext}}$, due to contributions from the dipolar field, the hyperfine contact interaction, the Lorentz field, and the demagnetization field. In a transverse field experiment, one is often interested in the difference between the two, $\boldsymbol{B}_\mu - \boldsymbol{B}_{\mathrm{ext}}$, but measured along $\boldsymbol{B}_{\mathrm{ext}}$. This is because the component of $\boldsymbol{B}_\mu - \boldsymbol{B}_{\mathrm{ext}}$ measured perpendicular to $\boldsymbol{B}_{\mathrm{ext}}$ makes very little difference to the precession frequency. The Knight shift K is then defined by

$$K = \frac{(\boldsymbol{B}_\mu - \boldsymbol{B}_{\mathrm{ext}}) \cdot \boldsymbol{B}_{\mathrm{ext}}}{B_{\mathrm{ext}}^2}, \tag{5}$$

and, hence, $B_\mu \approx (1+K)B_{\mathrm{ext}}$. The dipolar field from ordered moments contributes to K, but even in the paramagnetic state, the moments can become partially polarized in an applied field and take the value

$$\boldsymbol{m}_j = \frac{\underline{\boldsymbol{\chi}}\boldsymbol{B}_{\mathrm{ext}}\mathscr{V}_{\mathrm{c}}}{\mu_0}, \tag{6}$$

where $\mathscr{V}_{\mathrm{c}}$ is the volume per magnetic ion, and $\underline{\boldsymbol{\chi}}$ is the magnetic susceptibility tensor. Hence,

$$\boldsymbol{B}_{\mathrm{dip}} = \underline{\mathscr{D}}\underline{\boldsymbol{\chi}}\boldsymbol{B}_{\mathrm{ext}}, \tag{7}$$

where $\underline{\mathscr{D}} = \frac{\mathscr{V}_{\mathrm{c}}}{\mu_0}\sum_j \underline{\boldsymbol{D}}_j$ is the total dipolar tensor. Similarly, the contact hyperfine interaction $\boldsymbol{B}_{\mathrm{hf}}$ is given by

$$\boldsymbol{B}_{\mathrm{hf}} = \underline{\mathscr{A}}\underline{\boldsymbol{\chi}}\boldsymbol{B}_{\mathrm{ext}}, \tag{8}$$

where $\underline{\mathscr{A}}$ is the analogous hyperfine tensor. The contact coupling is usually independent of the field direction, and so this can be written as a scalar in the majority of cases. This provides us with all we need to model the effect of rotating a single crystal in a constant magnetic field and predicting the Knight shift for a particular muon site, the anisotropy of the dipolar coupling resulting in angle dependence, while the contact interaction gives an angle-independent contribution.

Another experimental test of the validity of a candidate muon site can be obtained using the contribution of nearby nuclear dipoles to the decay rate of a transverse-field precession measurement. The damping of the precession signal arises from contributions from nearby nuclear dipoles, which are not ordered, but sometimes add and sometimes subtract from the applied field. In a transverse field measurement, the broadening is given at short times by a Gaussian

relaxation function $\exp(-\sigma^2 t^2/2)$, where the parameter σ^2 (also known as the second moment M_2 in NMR) is given by[4,23–25]

$$\sigma^2 = \frac{1}{3}\left(\frac{\mu_0}{4\pi}\right)^2 \hbar^2 \gamma_\mu^2 \sum_i \gamma_i^2 I(I+1)\frac{(1-3\cos^2\theta_i)^2}{r_i^6}. \quad (9)$$

This depends on the spin I of the nearby nuclei, and their position r_i and gyromagnetic ratio γ_i. This depolarization rate is angle-dependent (θ_i is the angle between the applied field and the vector between the muon and the nucleus), so this broadening can be measured experimentally. In the case of a zero-field measurement, the relaxation takes on the Kubo–Toyabe form with a value of Δ^2 given by

$$\Delta^2 = \frac{1}{3}\left(\frac{\mu_0}{4\pi}\right)^2 \hbar^2 \gamma_\mu^2 \sum_i \gamma_i^2 I(I+1)\frac{(5-3\cos^2\theta_i)}{r_i^6}, \quad (10)$$

which again can be checked by an experiment. Moreover, in some fortunate cases (particularly fluorides), the zero-field signal from the nuclei contains much more structure than a simple Kubo–Toyabe relaxation (which is derived from an assumption of a Gaussian-distributed random distribution of local field components). In those cases, there is much more information to go on to deduce the muon site and understand the local environment.

III. DFT+μ

The methods described in Sec. II can all be useful in guessing and experimentally checking the muon site. However, electronic structure calculations are now proving to be extremely reliable as an *ab initio* technique for deducing muon sites, as well as for calculating the resulting distortion induced by the presence of the muon. In this section, we first review briefly the ideas behind density functional theory (DFT) (for an excellent introductory review, see the book by Giustino[26]) and then describe how DFT can be implemented for muon site calculations.

A. Density functional theory

The many body wave function is a complex object to evaluate and store (making demands on memory size that grow exponentially with system size, resulting in one of the pioneers of the subject even doubting whether the many body wave function is a legitimate scientific concept for systems of more than a handful of atoms![14]). The approach taken in DFT[14,26] is to dispense with the many body wave function and instead deal with the functional $E[n(\boldsymbol{r})]$ whose output is the ground state energy of the N-electron system and whose input is the electron density function $n(\boldsymbol{r})$. The electron density is not a function of all of the coordinates of all of the electrons; it is simply a function of the three position coordinates $\boldsymbol{r} = (x, y, z)$; thus, we treat the electron density as a fluid and forget that the electrons are really individual quantum objects obeying antisymmetry conditions. The functional is therefore a quantity averaged over $3N-3$ of the degrees of freedom of the N-particle wavefunction. It seems surprising that we can make such a severe simplification and still compute the energy of a system, but that this is possible is the result of the two Hohenberg–Kohn (HK) theorems.[27]

The first HK theorem establishes a one-to-one correspondence between an external potential $V(\boldsymbol{r})$ and the ground state electronic density $n(\boldsymbol{r})$. It can be proved that the ground state density $n(\boldsymbol{r})$ uniquely determines the potential, and hence all of the properties of the system. So, for example, the ground state energy E, can be written as a unique functional of the electron density $n(\boldsymbol{r})$ via an expression of the form

$$\begin{aligned} E[n(\boldsymbol{r})] &= T[n(\boldsymbol{r})] + E_{ee}[n(\boldsymbol{r})] + E_{en}[n(\boldsymbol{r})] \\ &= F[n(\boldsymbol{r})] + \int d^3r\, n(\boldsymbol{r}) V_{en}(\boldsymbol{r}), \end{aligned} \quad (11)$$

where, in the final line of Eq. (11), we have separated out the electron-nuclear part of the energy E_{en} and have written the rest as $F[n(\boldsymbol{r})] = T[n(\boldsymbol{r})] + E_{ee}[n(\boldsymbol{r})]$, which is a functional encoding all of the purely electronic contributions to the energy. If we have access to $E[n(\boldsymbol{r})]$, then we might be able to solve the problem of finding the electronic configuration corresponding to it by minimizing E with respect to the electron density n. That is, we continually adjust the function $n(\boldsymbol{r})$ until we find a form that gives us the lowest-energy electron density E. Is this a safe strategy? The second HK theorem tells us that it is.

The second HK theorem states that $E[n(\boldsymbol{r})]$ gives the lowest energy if, and only if, the input density $n(\boldsymbol{r})$ is the true ground state electron density. If we do not use the true density, then we obtain an upper bound on the ground state energy. Thus, the idea is to minimize the functional $E[n(\boldsymbol{r})]$ with trial functions $n(\boldsymbol{r})$, and if we find the actual minimum, then we will have the true electron density. There is, however, a problem, in that we do not actually know the exact form of the electron functional $F[n(\boldsymbol{r})]$. So, how do we find it?

A major simplification of the calculation of the electron density is made if we use the Kohn–Sham formulation,[28] the idea of which is to reformulate the problem by replacing the interacting system of many electrons by a non-interacting system of many electrons constrained to have the same electron density. Thus, the idea is to approximate the interacting kinetic energy $T[n(\boldsymbol{r})]$ of the N interacting particles by the kinetic energy $T_s[n(\boldsymbol{r})]$ of N non-interacting particles with the same density $n(\boldsymbol{r})$. We also extract from $F[n(\boldsymbol{r})]$ the Hartree component $U[n(\boldsymbol{r})]$. The Hartree component is simply the classical Coulomb interaction between regions of charge density and can be easily written in terms of $n(\boldsymbol{r})$. We then write

$$F[n(\boldsymbol{r})] = T_s[n(\boldsymbol{r})] + U[n(\boldsymbol{r})] + E_{xc}. \quad (12)$$

We have, therefore, bundled up our remaining ignorance into the functional E_{xc}, known as the exchange-correlation energy. To summarize, the HK theorems tell us we can find the ground state energy by minimizing a functional $E[n(\boldsymbol{r})] = F[n(\boldsymbol{r})] + \int d^3r\, V_{en}(\boldsymbol{r}) n(\boldsymbol{r})$ with respect to the density $n(\boldsymbol{r})$. The KS formulation, with its replacement of the interacting system with an equivalent non-interacting one, allows us to say that this minimization will be equivalent to a simpler procedure where we minimize the total energy of a non-interacting system subject to an effective potential V_s, whose form is

$$V_s(\boldsymbol{r}) = V_{en}(\boldsymbol{r}) + V_H(\boldsymbol{r}) + V_{xc}(\boldsymbol{r}). \quad (13)$$

The first term in the effective potential represents the electron-nuclear potential, the second the Hartree interaction, and the third the exchange-correlation potential. The end result of the KS approach is that we can solve the ground state density for the interacting system by first solving the Schrödinger equation for a single particle in an effective potential, using the set of KS equations defined as

$$\left[\frac{\hat{p}^2}{2m} + V_s(\boldsymbol{r})\right]\phi_i(\boldsymbol{r}) = \varepsilon_i\phi_i(\boldsymbol{r}). \quad (14)$$

The solutions of these KS equations give a set of KS wavefunctions and energy levels labeled by i. These states are filled up by the set of available electrons, and the density can be constructed from these non-interacting wavefunctions as $n(\boldsymbol{r}) = \sum|\phi_i(\boldsymbol{r})|^2$, where the sum runs over the occupied states.

Although we now have a set of single-particle problems to solve, we do not actually know the potential. Our ignorance has two aspects: the first is the functional form of V_{xc}, the second is that the Hartree potential V_H and the exchange correlation potential V_{xc} both depend on $n(\boldsymbol{r})$, the solution to the problem, which in turn is constructed from $\phi_i(\boldsymbol{r})$. The first problem can be addressed by approximating V_{xc}, using, for example, the local density approximation (LDA)[28] or some more sophisticated approach.[29–31] We then solve the equations iteratively: (i) an initial guess is first made of $n(\boldsymbol{r})$, and the potential V_s is computed; (ii) the single-particle wavefunctions are computed; and (iii) the set of occupied ϕ_i is used to compute $n(\boldsymbol{r})$, and then we start again by returning to step (i) and recalculating the potential. This procedure is repeated until some suitable convergence criterion is reached.

Central to the use of DFT is the Born–Oppenheimer (BO) approximation. This approximation makes use of the fact that atomic nuclei are much heavier than electrons, and therefore that the energy scale for the electronic part of the wavefunction is significantly larger than that of the nuclear part of the wavefunction, allowing these to be separated. The approximation, therefore, allows us to treat the atomic positions as parameters of an electron-only Hamiltonian that obeys a Schrödinger equation. The Born–Oppenheimer approximation basically clamps the nuclei at given fixed positions and the appropriate electron wavefunction is the one corresponding to this clamped nuclear configuration. However, nothing tells us whether the configuration of nuclei we specify is an equilibrium one. Since one of our main purposes in using DFT is finding the details of the nuclear structure that accommodates the muon, we must repeat our calculation of the electronic density for different nuclear structures until a global minimum in the ground state energy has been found. To do this, we allow the nuclei to move under the effect of forces, until these forces become small enough that we judge the system is at equilibrium. This process is called a geometry optimization (or a relaxation of the structure).

The BO approximation will be important in applying DFT techniques to a crystal containing a muon impurity. The muon is treated as a nucleus (a reduced-mass hydrogen) which, like all nuclei within BO, is clamped into position. The fact that the muon is 1/9 the mass of a proton and, therefore, somewhere between a nucleus and an electron, ultimately limits the applicability of the technique, as we discuss in Sec. IV F.

B. Adding the muon

The DFT + μ technique is based around using DFT to optimize the geometry of a material along with a muon impurity using methods developed for first-principle calculations of defect states.[32] In practice, we can start by randomly assigning an initial muon site in a unit cell of the target material and relaxing the structure by allowing both the muon and the atoms in the crystal to adjust their positions via repeated iteration until the forces on them are reduced below the threshold. We then evaluate the total energy of the final relaxed configuration. For crystalline materials, we generally use DFT codes that assume periodic boundary conditions. Since the muons in a μSR experiment are implanted in the ultra-dilute limit, to ensure the boundary conditions never result in muon–muon interactions, we usually specify the structure via a supercell, containing a number of unit cells and a single muon. The charge state of the muon is determined by the overall charge of the defect [+1 for diamagnetic and neutral, zero for paramagnetic states], which is fixed initially; note that for the diamagnetic case, a uniform, smeared-out Hartree-like compensating charge is added to the supercell to ensure overall neutrality,[33–35] and the final charged state of the impurity is to be determined by the final relaxed configuration.

The geometry optimization is repeated for several other randomly chosen initial muon sites, with the lowest total energy of the relaxed structure yielding the most likely muon site, as well as providing an estimate for the structural distortion the muon introduces. Often this procedure will lead to a range of candidate muon sites being produced. It is then necessary to form these into clusters of roughly equivalent sites, which is most efficiently done by making use of the underlying symmetry of the unperturbed material's structure, along with some assumptions about the nature of the distortion and the energy ranges of sites that are likely to be realized. The method has proved extremely successful, providing results which are in quantitative agreement for cases in which the muon site can be independently verified (for example, ionic fluorides provide a valuable test-bed for evaluating the method because of the quantum coherent oscillations produced in F–μ–F states,[17] see Sec. IV A).

Since this procedure is rather well defined for most systems, it is possible to create simple software solutions that allow it to be carried out automatically. The first calculations[10,11] utilized bespoke programs calling the open-source electronic structure code QUANTUM ESPRESSO.[36] Recently, some examples have started to become available for general use. MuFinder[37] is a tool that enables users to carry out muon-site calculations via a simple graphical user interface (GUI). The procedure for calculating muon sites, by generating initial muon positions, relaxing the structures, and then clustering and analyzing the resulting candidate sites, can be done entirely within the GUI. The software was originally configured to make use of the plane wave electronic structure code CASTEP.[38] Once candidate muon sites have been determined, the local magnetic field at the muon site can then also be computed within the program, making use of the Magnetic structure and mUon Embedding Site Refinement (MuESR) software,[39] allowing the connection between the muon sites obtained and experiment to be made. Alternative software tools are also available, including one based on a combination of *ab initio* random structure searching (AIRSS) and machine learning.[40] Here, AIRSS is a general scheme for randomly generating possible structures a system can adopt and then introduce biases based on chemical, experimental, and/or symmetry grounds.[41]

The method described so far can be quite computationally costly, owing to the need for many iterations of the optimization procedure to relax the structure. In view of this, an alternative scheme is the unperturbed electrostatic potential (UEP) method, in which the charge density of the host material obtained from a DFT calculation is used, unperturbed by the presence of the muon. This provides an estimate

of the Coulomb force acting on each of the μ^+ in the initial muon-containing structures. This potential is a direct output of the DFT calculation, being the opposite of the Coulomb potential experienced by electrons, and its minimum represents the candidate site where the muon feels zero force. Although approximate, the UEP method is extremely fast and works reasonably well in materials in which atomic displacements do not play a major role in stabilizing a diamagnetic muon site.[42]

To further reduce computational cost, semi-empirical methods can be employed, which rely on simplifying approximations and parameterizations to allow more efficient computations. Hartree–Fock (HF) theory[43] was much used before DFT became established. For speeding up HF calculations, a useful series of semi-empirical methods were developed in which a set of empirical parameters is derived for each chemical element treated by the method. This is done by optimizing against a training set of molecular data, which includes properties such as geometry, ionization energy, and electric dipole moment, and is generally limited to light atoms and molecular materials.[4] In view of the success of the efficient HF semi-empirical approach, attempts were made to apply similar semi-empirical ideas to the DFT calculation framework. This led to the method known as density functional tight binding (DFTB), which focuses on parametrizing the interactions between pairs of atoms.[44] The DFTB method is relatively fast, since each stage in the geometry relaxation only requires a single diagonalization of the energy matrix, rather than the iterative self-consistent-field loop of a usual DFT calculation. Although the semi-empirical methods are useful for rapidly obtaining geometries for a subset of problems, such as muoniated molecular radicals, they are not able to produce accurate spin structures. Thus, in order to produce a reliable spin distribution and corresponding hyperfine parameters, it is necessary to follow on with a single-point DFT calculation after the semi-empirical geometry optimization.[4]

IV. EXAMPLES

The location of the muon site in a solid is chiefly determined by the electrostatic interactions of the positively charged muon and its surroundings. In metals, we expect to find bare muons (often called diamagnetic muons), uncoupled from unpaired electron density. In insulators, there is also the possibility of forming muonium (Mu): a bound state of an electron and muon with a binding energy of 13.54 eV (*in vacuo*). However, our interest below is mostly in bare muons. We expect a stopped bare muon to be self-trapped by its own local distortion to the lattice,[4] such that (classically) it sits at the bottom of an electrostatic potential well. The energy scales chiefly at play determining muon sites are therefore electrostatic ones of order 0.1–10 eV. This large range of scales, which is often reflected in the energy differences between candidate muon-containing structures found using DFT follows from that found in the cohesive energies of different types of solid, from molecular crystals (of order 0.1 eV/molecule), through metals (1 eV/atom), to insulators (10 eV/atom).[45] Such scales are well described by electronic-structure methods such as DFT. Its worth noting that magnetic interactions, whose energy scales are typically determined by interactions of order tens of millivolts and below, are rather smaller still. So while the electronic state of a material, and the consequent distribution of electron density, will likely affect the muon-stopping state, the magnetic state of a material (and the consequent distribution of electron spin density) is unlikely to determine the muon site.

A. Fluorides

Ionic fluorides were one of the first systems[10,11] to be studied using DFT + μ. This is because the muon site in fluoride systems can be identified using the characteristic experimental signature of an F–μ–F state.[17] Even though there is no electronic magnetism in many of these compounds, a clear and rather complex precession signal was observed, and they have some rather special properties: (i) fluorine is extremely electronegative and thus attractive to the positively charged muon, (ii) F^- has a very small ionic radius (so that the muon sits very close), (iii) the fluorine nucleus has spin one-half (so that any relaxation retains a simple, yet characteristic, time dependence), and (iv) the fluorine nucleus has a large nuclear moment, associated with an isotope which occurs with 100% abundance (so that all states behave the same). It was recognized that the effect could be explained if a muon stops between two fluorine ions to form what is known as an F–μ–F state. This state can be described by the Hamiltonian $\mathscr{H}$ given by

$$\mathscr{H} = \mathscr{H}_{\mu\mathrm{F}} + \mathscr{H}_{\mathrm{FF}}, \tag{15}$$

the sum of two terms expressing the dipolar interaction between the muon and the fluorine nuclei,

$$\mathscr{H}_{\mu\mathrm{F}} = \frac{\mu_0}{4\pi}\sum_{i=1}^{2}\frac{\hbar^2\gamma_\mu\gamma_\mathrm{F}}{r_i^3}\left[\boldsymbol{S}_\mu\cdot\boldsymbol{S}_{\mathrm{F}i} - \frac{3(\boldsymbol{S}_\mu\cdot\boldsymbol{r}_i)(\boldsymbol{S}_{\mathrm{F}i}\cdot\boldsymbol{r}_i)}{r_i^2}\right], \tag{16}$$

and the dipolar interaction between the fluorine nuclei,

$$\mathscr{H}_{\mathrm{FF}} = \frac{\mu_0}{4\pi}\frac{\hbar^2\gamma_\mathrm{F}^2}{r_{\mathrm{FF}}^3}\left[\boldsymbol{S}_{\mathrm{F}1}\cdot\boldsymbol{S}_{\mathrm{F}2} - \frac{3(\boldsymbol{S}_{\mathrm{F}1}\cdot\boldsymbol{r}_{\mathrm{FF}})(\boldsymbol{S}_{\mathrm{F}2}\cdot\boldsymbol{r}_{\mathrm{FF}})}{r_{\mathrm{FF}}^2}\right]. \tag{17}$$

If we ignore the interaction between the two fluorine moments, then eigenvalues are -1, $\frac{1-\sqrt{3}}{2}$, 0, and $\frac{1+\sqrt{3}}{2}$, all in units of $\hbar\omega_\mathrm{d} = \mu_0\hbar\gamma_\mu\gamma_\mathrm{F}/(4\pi r^3)$ and twice-repeated, so the energy levels are four doublets. The polycrystalline average polarization is then given by an analytical form

$$\langle P_z(t)\rangle = \frac{1}{2} + \frac{1}{6}\sum_{i=1}^{3} a_i\cos(\alpha_i\omega_\mathrm{d}t), \tag{18}$$

with $a_1 = 1$, $a_2 = 1 - \frac{1}{\sqrt{3}}$, $a_3 = 1 + \frac{1}{\sqrt{3}}$, $\alpha_1 = 1$, $\alpha_2 = \frac{3-\sqrt{3}}{2}$, and $\alpha_3 = \frac{3+\sqrt{3}}{2}$. If the interaction between the two fluorine moments is also included then the factors in this expression change a little bit (and the expression does not look as pretty). Nevertheless, the form of the oscillatory signal provides information concerning the nature of the interaction (whether with one fluorine, or two, and whether the F–μ–F bond is straight or bent), and the timescale of the oscillatory signal is set by ω_d, and hence by r, so that the muon-fluorine bond length can be accurately measured. This provides crucial quantitative information on the muon site and its local distortion, allowing a rigorous test of the accuracy of the DFT +μ calculations.

The oscillations in the muon polarization described in Eq. (18) have been observed experimentally in many inorganic fluorides,[17,46] fluoropolymers,[47–49] and fluorine-containing molecular magnets.[50] DFT +μ calculations[10] in a variety of inorganic fluorides (LiF, NaF, CaF_2, BaF_2, and CoF_2) reveal a linear F–μ–F state with a F–F internuclear distance between 2.31 and 2.36 Å, whose range includes 2.36 Å, the measured distance of the $(FHF)^-$ molecular bifluoride ion in

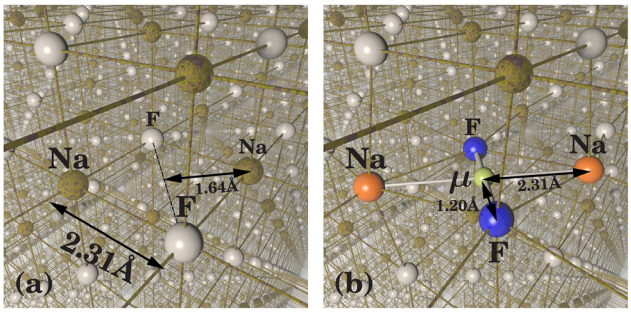

FIG. 1. (a) The crystal structure in NaF. (b) After implantation of the muon, two nearby fluorine ions are pulled in and two nearby sodium ions are pushed out. Adapted with permission from J. Wilkinson and S. J. Blundell, Phys. Rev. Lett. **125**, 087201 (2020). Copyright 2020 American Physical Society.[52]

vacuum.[51] The bifluoride ion has various vibrational modes (e.g., a bending mode of frequency around 1290 cm^{-1}), but the calculated modes for F–μ–F are around a factor of three larger[10] (due to the muon mass being approximately one ninth of the proton mass). This results in the muon in a F–μ–F state having a zero-point energy of ≈0.8 eV, considerably larger than the value of ≈0.3 eV for the proton in the bifluoride ion.[10] We will return to this point in Sec. IV F.

The rigidity of the F–μ–F bond will introduce a distortion into the crystal. For example, in CaF_2, the F–μ distance is found by experiment to be 1.172 Å (with the DFT +μ calculation giving 1.134 Å), but this value is much lower than $a/4 = 1.362$ Å, the distance between the muon site and the fluorine ion in its undistorted position, demonstrating a significant distortion.[52] The same effect in NaF is illustrated in Fig. 1. In the undistorted structure, each ion sits 1.64 Å from the site of the muon; following implantation, the distance from the muon to the nearest-neighbour fluorine (sodiuum) ion becomes 1.20 Å (2.31 Å). The results of these DFT +μ calculations are in excellent agreement with experimental results for which the complex precession signals due to the dipolar couplings with all nearby nuclei can now be calculated and high-statistics measurements have now been performed.[52]

This approach has now been extended to other fluorides, including YF_3 (see Fig. 2) and α-PbF_2; in the latter compound, the μSR data and analysis provide evidence for a $Mu^- = \mu^+e^-e^-$ stopping site in an anion Frenkel defect.[53] Although fluorine is the most ideal ion for exploring these effects, it is not the only one. μSR data obtained on V_3Si shows evidence for quantum coherent oscillations, which can be related to a V–μ–V state.[54] These experiments highlight the extreme sensitivity of the entangled states to the local structural and electronic environments, which, in the case of these A15 compounds containing V (and also Nb), emerges through the quadrupolar interaction with the electric field gradient. This demonstrates that positive muons, usually thought of as a purely magnetic probe, can also be deployed as quantum sensors to measure structural and charge-related phenomena.[54]

B. Magnetism

Magnetism remains a key research area for μSR, and many applications of the DFT + μ techniques have concentrated on systems that are magnetically ordered. Here, a knowledge of the muon site tells us which magnetic fields are causing the time-evolution of the muon's

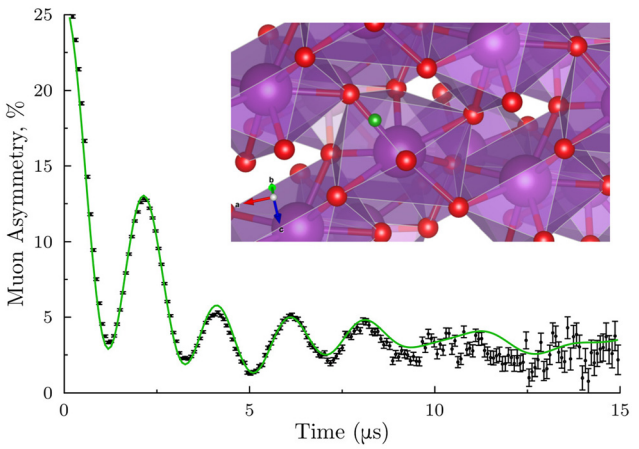

FIG. 2. μSR experimental data on YF_3 with the fitted muon polarization using the muon site obtained by DFT +μ. This site is displayed on the YF_3 crystal structure in the inset. Adapted with permission from Wilkinson *et al.* Phys. Rev. B **104**, L220409 (2021). Copyright 2021 American Physical Society.[53]

spin, potentially giving us access to more information on the local magnetic field distribution and its dynamics.

A simple, topical example is found in materials adopting the double-perovskite structure exemplified by antiferromagnetic Sr_2FeOsO_6.[55] In this system, the muon site is found from DFT to be approximately 1 Å from an oxygen atom in the basal plan of the oxygen octahedra surrounding the Os ions, validating the rule of thumb that such sites close to O^{2-} ions are most likely in oxides. In this case, the site is consistent with the dipole-field map computed for the known magnetic structure, giving confidence that the DFT-derived site is likely the one realized. Other ionic systems in which DFT+μ calculations show that the muon occupies a site close to the anion include the honeycomb system[56] α-$RuCl_3$, and the spin-Jahn-Teller antiferromagnets[57,58] $CoTi_2O_5$ and $FeTi_2O_5$. A similar approach applies in the case of the ferromagnet $Nd_2Fe_{14}B$, where the muon site is identified [the 8i site (0.6745, 0.8838, 0)] near the square base of a $NdFe_3B$ pyramid, leading to a quantitative measurement (using the observed μSR precession frequencies) of the moment on the Nd and Fe atoms.[59]

More stringent tests of DFT-computed sites are found in materials with more complicated, often noncollinear, magnetic structures and/or hyperfine contributions. The helimagnet MnSi has been the subject of several illuminating investigations of its properties using muons[60,61] and provides a good example of site-determination in a more complicated magnetic system, In this material, the muon site computed using DFT methods (shown in Fig. 3) is consistent with the symmetry properties derived from Knight-shift measurements, and also with the very restrictive details of the complicated magnetic structure of the material.[60] This information proved very useful in providing a complete analysis of the measured μSR spectra in terms of a magnetic structure and hyperfine interaction,[60] that did not require the invocation of a more exotic muon stopping state that had been previously suggested.[62]

Noncollinear magnetism magnetic structures are especially relevant to the study of skyrmion systems. Skyrmions[64] are vortex-like

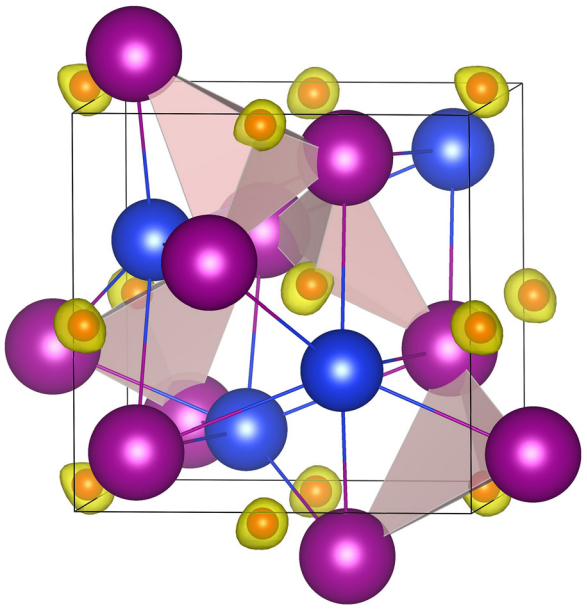

FIG. 3. The muon site in MnSi is found experimentally to be at $(0.532, 0.532, 0.532)$ (indicated by small circles at crystallographically equivalent sites). These positions are enclosed by the regions where the unperturbed electrostatic potential computed by DFT takes a minimum. Reproduced with permission from Amato *et al.*, Phys. Rev. B **89**, 184425 (2014).[60] Copyright 2014 American Physical Society.

magnetic excitations found in a growing number of magnetic materials. These include MnSi, which hosts Bloch skyrmions. Another example skyrmion compound, this one hosting Néel skyrmions, is GaV_4X_8 ($X = S$, Se). Structural relaxations of a supercell of GaV_4S_8[63] reveal four distinct muon sites (Fig. 4). Three of these (labeled I–III) involve the muon sitting close to a single S atom. A fourth site (site IV) has the muon closer to V atoms and is the highest energy site. In the lowest energy site (site I), the muon sits between two S atoms, in the plane defined by three S atoms within V_4S_4 units. The two μ^+–S distances are unequal (1.4 and 2.0 Å) with greater electron density found between the muon and the nearest S atom. This site is therefore best described in terms of the muon forming a μ^+–S bond (rather than an S–μ^+–S state), though the presence of a second nearby S atom does seem to stabilize this geometry. Two further sites involve the muon sitting close to a single S atom.

Perhaps, the most pressing problem with the DFT + μ method is determining which sites are actually realized given an energy-ordered list of candidate states. This problem is particularly relevant for the results of analogous calculations for GaV_4Se_8. These give stopping sites (labeled 1–4 in the order of ascending energy) that are similar to those calculated for GaV_4S_8, with three of the four sites involving the muon sitting close to a Se atom (sites 2–4) and a site in which the muon sits above a face of a V_4Se_4 unit (site 1). However, the ordering of sites is inverted in the Se case, compared to the S-containing series. In particular, the cube face site (site 1), which corresponds to the highest energy stopping site for GaV_4S_8, is the lowest energy site for GaV_4Se_8. Although the difference in energy ordering is interesting, without access to a method to compute the capture cross section for each site, the interpretation of this information remains an open question.

So far we have seen examples of the commonly encountered cases of sites near fluorine and near oxygen. An interesting case of a system where both sites near oxygens and fluorines are predicted is barlowite, a frustrated magnet kagome antiferromagnet with formula $[Cu_4(OH)_6FBr]$.[65] In this system, DFT suggests two distinct classes of muon stopping site. The first localizes ≈1.0 Å away from the oxygen atoms in the hydroxide groups that connect the Cu^{2+} ions within the kagome layers. This forms a triangular μ-OH complex, with the muon-proton distance of 1.54 Å in the lowest-energy sites. In the second class, muons localize near the fluoride anions in between the kagome layers, with a μ–F separation of 1.1 Å. These latter sites lie at substantially higher energies above the lowest energy sites in the calculations (≈1 eV). Although this suggests, on purely energetic grounds, that the formation of μ–F complexes in barlowite is unlikely compared to μ-OH. However, the measured spectra in the paramagnetic regime show clear dipole–dipole oscillations consistent with a μ–F complex,

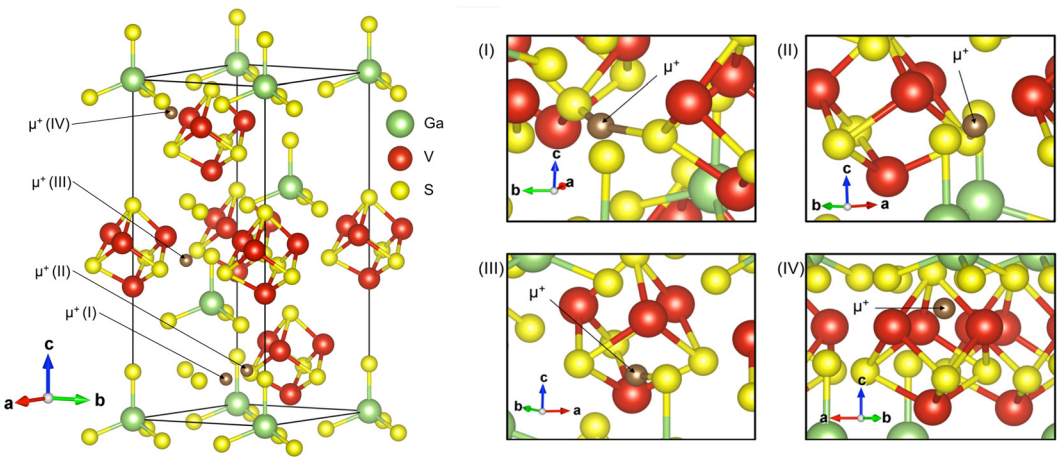

FIG. 4. Left: the four classes of muon stopping site determined for GaV_4S_8. Right: local geometry around the muon for each of the four classes of muon stopping site in GaV_4S_8. The sites are numbered in order of increasing energy. Adapted with permission from Franke *et al.*, Phys. Rev. B **98**, 054428 (2018). Copyright 2018 American Physical Society.[63]

implying that during the stopping process, muons are indeed captured in these latter potential minima.

The study of H-like defects in semiconductors and insulators using first-principles methods is a mature field,[32,35,66] and understanding the analogous muon-like states is clearly related.[67,68] A recent development has come from the suggestion that in certain oxides, such as Cr_2O_3, the muon can form a charge-neutral complex composed of a muon and an electron polaron.[69] Cr_2O_3 contains Cr^{3+} ($3d^3$) ions, but the idea is that the μ^+ binds to an oxygen anion but an excess electron localizes on an adjacent Cr ion, changing its charge state to Cr^{2+} ($3d^4$), which is Jahn–Teller active, resulting in a Jahn–Teller polaron. The existence of this state is supported by first-principles calculations, and an analogous effect has been proposed[70] for Fe_2O_3.

C. Superconductivity

An important use of muon in superconducting materials is the investigation of the vortex lattice in type-II superconductors, where the muon can be used to measure the penetration depth. In such measurements, the muon site is often of secondary importance since the length scale of the vortex state is large on the scale of the underlying unit cell, so the muons effectively probe the whole of the flux lattice, whatever their stopping site in the crystal. However, the physics of unconventional superconductors is inextricably bound up with magnetic phenomena (and sometimes questions of phase separation and coexistence), and so in μ^+SR studies of materials showing unconventional superconductivity, it is usually absolutely necessary to have knowledge of the muon stopping state.

In the cuprate superconductors, it has been thought for a long time that the muon site will be about 1 Å away from an oxygen anion.[15] A recent study of muon sites in La_2CuO_4 has concluded that most muons stop near the apical oxygen, but there are two additional sites that also receive a tiny fraction of muons.[71] Iron-based superconductors provide another informative example of an unconventional superconducting series of materials.[72,73] The DFT calculation allows a straightforward identification of the muon site using the UEP approach. In the case of the 1111 structure, this allows the identification of three sets of potential minima shown in Fig. 5. Similar results have been obtained for[74] UTe_2.

One area where μSR has proven important is in attempts to determine instances of time-reversal symmetry breaking (TRSB) in superconducting systems, since this can provide a tight constraint on the symmetry of the superconducting gap.[75] The assignment of TRSB is made through the appearance of spontaneous magnetic fields found using μSR measurements. (Importantly, this effect is absent for most superconductors.) The effects observed are frequently small, and sometimes only seen in muon measurements, and so it is natural to ask whether a muon-induced perturbation is a contributing factor to the observations. A recent DFT + μ study of these materials[75] suggests that the muon is an innocent probe of these materials. We shall concentrate on one candidate TRSB material: the layered perovskite superconductor Sr_2RuO_4.

In the lowest-energy muon site found for Sr_2RuO_4, the muon is bonded to an oxygen (O_2) with bond distance 0.973 Å, consistent with muon sites in other oxides including high-temperature superconducting cuprates and pyrochlores. The small muon-induced displacement vanishes rapidly as a function of distance from the muon site, such that significant distortions are observed only for atoms within 6 Å of the muon site. We can, therefore, conclude that there is little structural distortion, but what about a distortion to the physics at the next largest energy scale: the electronic structure? It is found that the dominant contribution to the electronic density of states (DOS) close to the Fermi energy is that from the Ru atoms. The effect of muon implantation on the projected DOS of the Ru atom closest to the muon site is shown in Fig. 6. There is an increase in the DOS at around 1 eV below the Fermi energy caused by small changes in the splitting of the Ru $4d_{zy}$ and $4d_{zx}$ states at the Fermi level, which are not observed for Ru atoms further away from muon. However, after summing the d-state contributions from all of the Ru ions in the supercell, the small state splitting is no longer resolvable. The projected density of states corresponding to the muon itself lies around 8 eV below the Fermi energy. Since this is very large interval in energy, it is highly unlikely the muon has any effect on the electrons near the Fermi energy and so these results suggest that the implanted muon does not have a significant effect on Sr_2RuO_4. A similar conclusion was reached for other TRSB systems investigated in this study.[75]

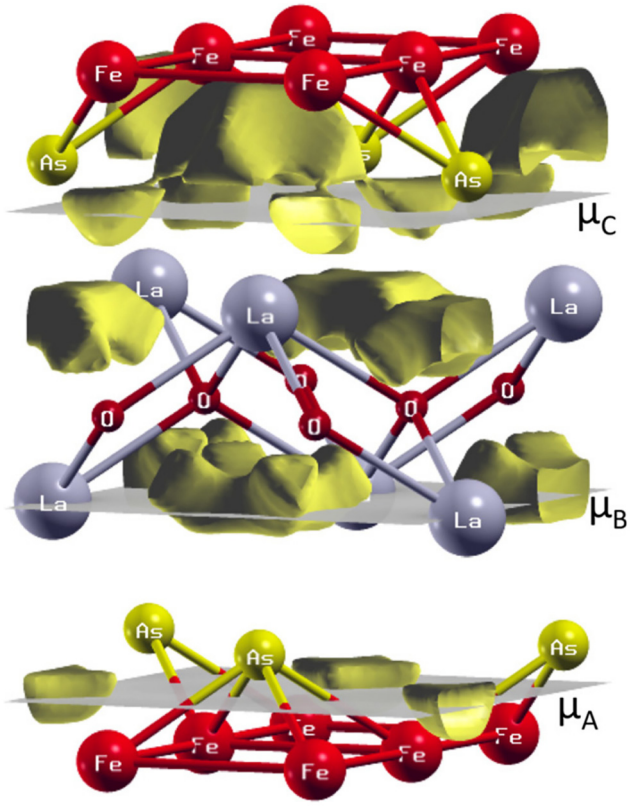

FIG. 5. Muon sites identified in the LaFeAsO unit cell. Gold-shaded areas represent the volume of zero point displacement for the muon. Reproduced with permission from De Renzi *et al.*, Supercond. Sci. Technol. **25**, 084009 (2012). Copyright 2012 Institute of Physics Publishing.[72]

D. Molecular systems

Muons are routinely used to elucidate the properties of molecular materials. These systems are attractive owing to their tunability, but

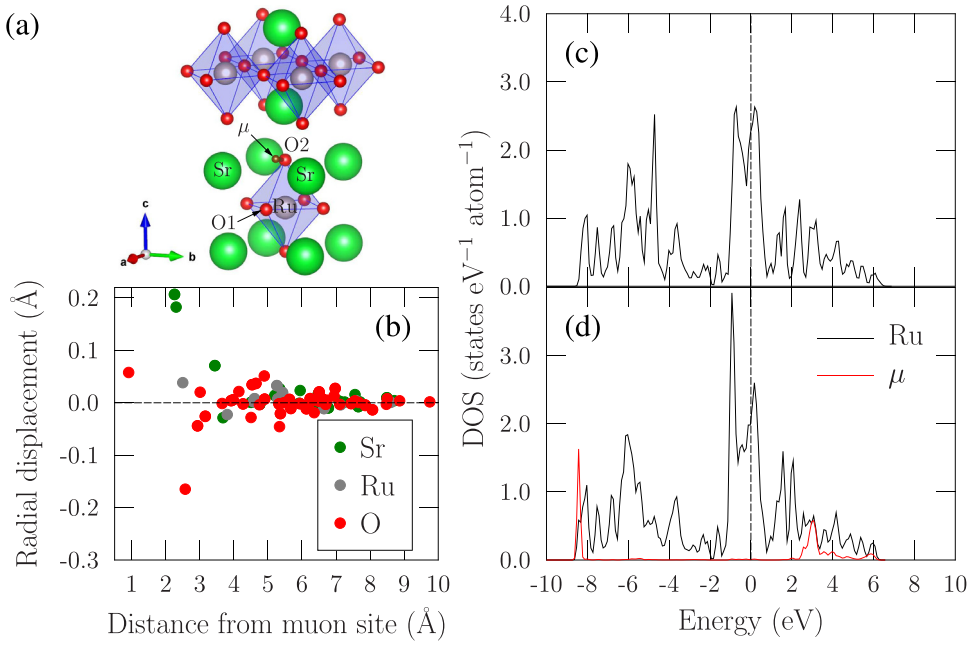

FIG. 6. The lowest-energy muon site in Sr_2RuO_4. (a) Local geometry of the muon site. (b) Radial displacements of atoms as a function of their distances from the muon site. projected density of states for the Ru atom closest to the muon site for the structures (c) without a muon and (d) with a muon. Energies are given with respect to the Fermi energy. Adapted with permission from Huddart *et al.*, Phys. Rev. Lett. **127**, 237002 (2001). Copyright 2001 American Physical Society.[75]

their chemical complexity regularly leads to questions about the nature of the muon stopping state. These materials are rather soft in comparison to their inorganic counterparts, and so we might expect that the muon-induced distortion could present a relatively large perturbation to the electronic or magnetic properties of the system.

One class of these materials are coordination polymer magnets, where a magnetic ion is linked via molecular ligands to form a low-dimensional magnet. These are of interest since the low-dimensional character often suppresses long-range magnetic order, reducing the size of the response of conventional measurement techniques owing to the small moment size and small change in entropy upon ordering. In these systems muons are often able to detect transitions that prove invisible to magnetic susceptibility or specific heat.

The staggered molecular spin chain [pym-Cu$(NO_3)_2(H_2O)_2$] (pym = pyrimidine), known as Cu-PM, is a good example.[76] Here, a magnetic order was detected using muons at $T = 0.23$ K. Three distinct classes of muon stopping site were determined (Fig. 7). Sites where the muon sits around 1 Å from an O atom in a nitrate group [Fig. 7(a)] or H_2O ligand [Fig. 7(b)] are the lowest and second lowest energy classes of sites, respectively. We also find candidate sites where the muon sits 1.0 Å from an N atom in a pym ligand [Fig. 7(c)], which are substantially higher in energy and result in larger local distortions to the crystal structure. These sites can be mapped to features in the ZF spectra by considering the dipolar fields resulting from candidate antiferromagnetic structures. From dipolar field calculations, one obtains fields of 9–40 mT/μ_{Cu} for the nitrate site, 57–63 mT/μ_{Cu} for the H_2O site, and 93–99 mT/μ_{Cu} for the N(pym) site, where μ_{Cu} is the ordered moment of the Cu^{2+} ions in Bohr magnetons. The relative size of the calculated fields for the H_2O and nitrate sites is consistent with the ratio between observed frequencies measured in the ordered regime. This assignment gives an estimate $\mu_{Cu} \approx 0.38\,\mu_B$ for the ordered moment.[76]

There have been claims,[77] supported by some experimental evidence,[78] that a muon implanted in some spin chains could form an unusual spin-singlet state, not unlike that found in the Kondo effect. However, results on materials such as Cu–PM and the linear chain

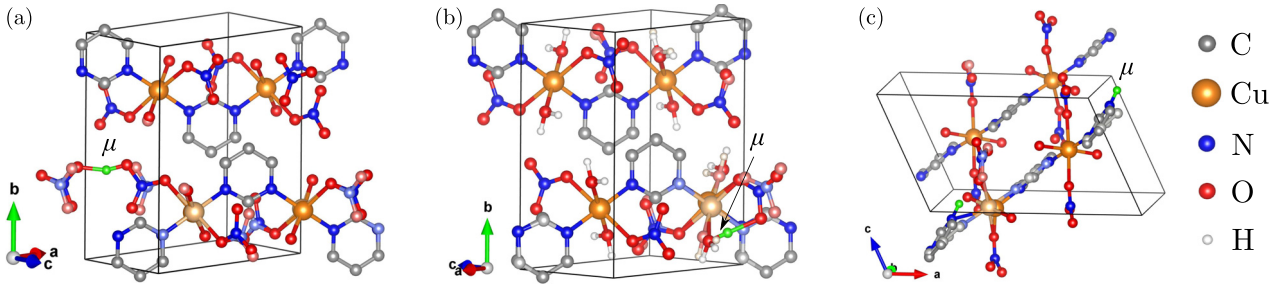

FIG. 7. Low-energy muon sites in Cu–PM. Lighter spheres represent the ionic positions in the unit cell without the muon. H atoms have been omitted for clarity where appropriate. (a) The nitrate site. (b) The H_2O site. (c) The N(pym) site. Reproduced with permission from Huddart *et al.*, Phys. Rev. B **103**, L060405 (2021). Copyright 2021 American Physical Society.[76]

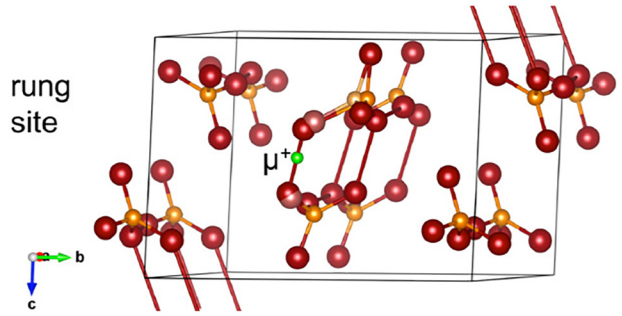

FIG. 8. Example muon site in the molecular spin ladder $(Hpip)_2CuBr_4$. Reproduced with permission from T. Lancaster *et al.*, New. J. Phys. **20**, 103002 (2018). Copyright 2018 Institute of Physics Publishing.[80]

$Cu(pyz)(NO_3)_2$,[79] do not provide evidence for the realization of these states. An example where a substantial muon-induced perturbation seems to be present is the molecular spin-ladder material $(Hpip)_2CuBr_4$,[80] where the muon forms states based on Br– μ–Br bonds. This state causes a sizeable local distortion to the atoms neighboring the muon and consequently to the electronic structure (Fig. 8). Although it might be feared that this would prevent the muon from faithfully measuring the properties of the material, this seems not to be the case as the magnetic phase diagram is determined by physics on a length scale that is very long compared to the muon and its distortion. As a result the transitions in the material are observed with μSR at the fields and temperatures found using other techniques.

An example of a rather different structure is the organic radical 2–(4,5,6,7-tetrafluorobenzimidazol-2-yl)-4,4,5,5-tetramethyl-4,5-dihydro-1*H*-imidazole-3-oxide-1-oxyl (F4BImNN),[81] which forms hydrogen-bonded chains and exhibits one-dimensional ferromagnetic exchange. Here, three energetically similar sites are predicted: (i) where the muon forms a covalent bond with the oxygen in the nitronyl nitroxide group (see Fig. 4), (ii) where the muon forms a covalent bond with the vacant nitrogen and hydrogen-bonds to the one oxygen in the nitronyl nitroxide group (this is the lowest energy site), and (iii) where the muon bonds to the other oxygen in the nitronyl nitroxide group. Interestingly, despite the presence of fluorine in this sytem, an F–μ–F state is not predicted.

E. Muon-induced distortions

This example of a spin-ladder material from Sec. IV D is a case where the muon-induced distortion likely leads to a probe state comprising both the muon and its surrounding perturbation that is nevertheless sensitive to the intrinsic properties of the material. However, it is natural to ask about other cases where the muon has a strong effect on its surroundings.

An important example of this was found in a family of quantum spin ices; a muon-induced change of the local crystal field dominates the measured response in a way that could be fully quantified,[82] demonstrating that the concerns raised above can be of critical importance. Spin ice materials are based on the pyrochlore structure and the physics of such pyrochlore materials, with the general formula $A_2B_2O_7$, it is strongly dependent on the crystal field surrounding the lanthanide cation A. Thus, the introduction of a muon into the structure could alter that crystal field and change the nature of the ground state.

This effect is realized in the material $Pr_2Sn_2O_7$, which exhibits quantum spin ice behavior.[83] Without the muon, the Pr^{3+} ion is surrounded by eight oxygen anions and adopts a doublet crystal field ground state, resulting in an effective spin-$\frac{1}{2}$ moment.[84] However, DFT $+\mu$ calculations imply that the presence of the muon [the site is identified as $(-0.013, 0.047, 0.203)$] distorts the local symmetry around nearby Pr ions. The largest effect is found to be an anisotropic distortion, with one Pr–O bond strongly rotated (bent) and another significantly extended (see Fig. 9). The net result is that the doublet ground state is split on each of the neighboring Pr cations has a singlet ground state. Then, via a hyperfine enhancement mechanism,[85,86] a distribution of static magnetic moments is produced in which the average moment size grows on cooling. The model (involving DFT $+\mu$ calculations of the distortion and crystal field calculations of the resulting Pr environments) produced quantitative agreement with the temperature dependence of the observed muon response, demonstrating the validity of this approach.[82] The Pr^{3+} ion has a non-Kramers ground state and so is particularly vulnerable to electrostatic perturbations. For the case of $Dy_2Ti_2O_7$, the Kramers doublet ground state of Dy^{3+} is unaffected by the muon, even though the muon site and resulting anisotropic distortion are pretty much identical to that shown in Fig. 9 for $Pr_2Sn_2O_7$.

F. Quantum effects

The DFT treatments described so far have assumed that the muon is a classical particle sitting statically at its equilibrium position. This is a consequence of the Born–Oppenheimer approximation where we make a clear distinction between the classical nuclei (including the positive muon, which is treated as a light proton) and the quantum electrons. However, this approach neglects quantum mechanical effects of muons and nuclei, such as zero-point motion, tunneling, and large zero-point energies (ZPEs). These can change the energetic ordering of muon sites, destabilize certain classical muon

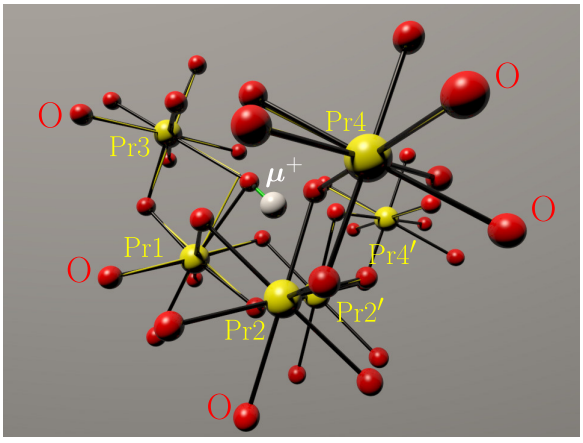

FIG. 9. Muon stopping site (white sphere) and atomic positions (oxygen ions are red, Pr ions are yellow, and Sn is suppressed) in the quantum spin ice $Pr_2Sn_2O_7$ as calculated by DFT $+\mu$. Bonds are shown as solid black lines, with the bonds of the unperturbed lattice (yellow lines) included for comparison. Pr ions are numbered in order of separation from μ with Pr1 being the closest. The pair Pr2 and Pr 2′ is equidistant from the muon, as are Pr4 and Pr 4′. Adapted with permission from Foronda *et al.*, Phys. Rev. B **92**, 134517 (2015). Copyright 2015 American Physical Society.[82]

sites, or cause several sites to merge into one if ZPE overcomes the potential-energy barriers between them. For nuclei, all of these effects are mass dependent and, therefore, especially pronounced for light particles such as the muon. The result is that, in reality, the muon wavefunction is expected to be spread over an appreciable volume in the material, rather than concentrated at a single point. All observable quantities such as muon coupling constants have, in principle, to be suitably averaged over the whole extended muon wavefunction, rather than sampled at a single classical point as in the Born–Oppenheimer approximation. The significant spatial extent of the wavefunction of the implanted muon is known to be relevant in many systems. Well-known examples are the quantum diffusion of muons in metallic systems such as copper or of muonium in insulating systems such as solid nitrogen.

Dealing with quantum effects is, of course, a difficult problem (DFT being a scheme invented to avoid this!) and so several approximations have been proposed and attempted. Perhaps, the simplest class of approximation is a harmonic one. This starts with a DFT calculation of the (Γ-point) phonon spectrum for the classical muon site geometry. An additional assumption often made is that, since muons are lighter than nuclei, muon zero point motion is adiabatically decoupled from the lattice over some relatively short length scale.

An example is, once again, provided by the fluorine states described in Sec. IV A. In vacuum, the linear F–μ–F anion has four vibrational modes: a symmetric stretch, bending (twofold degenerate), and an asymmetric stretch. In a solid, the twofold degeneracy of the bending mode is broken due to the symmetry of the site: in LiF, NaF, CaF_2, and BaF_2, there are two fundamentally inequivalent directions of bending; one is toward a neighboring cation and is shifted up in frequency, while the other direction is into a gap in the crystal structure and is shifted down in frequency. From the frequencies of these decoupled vibrational modes, we can estimate the zero-point energy (ZPE) of the muon. The strong bond in this case, combined with the small muon mass leads to a large ZPE for the F–μ–F center of 0.80 eV in vacuum. This is larger than the ZPE of any natural triatomic molecule (the ZPEs of H_2O and H_3^+ are 0.56 and 0.54 eV, respectively), demonstrating the importance of quantum effects in muon localization.[10]

More generally, the quantum muon problem can be addressed using a range of single-particle approximations where the muon sits in the potential of its surroundings and the Schrödinger equation is solved for the muon only. These schemes can be most easily addressed in two limits: weakly and strongly bound muons. In both of these, an effective single-particle potential is constructed from the total DFT energy. To do this, the muon is displaced from its classical site, while (i) keeping the nuclei fixed at the positions corresponding to the unperturbed muon site (in the weakly bound case), or (ii) letting the nuclei relax to new lowest-energy positions (in the strongly bound case), while keeping the center of mass of the system fixed.

An example of an attempt to apply these approaches is the case of α-N_2.[87] Here, the muon forms an extended electric-dipole polaron around a central, quantum-entangled $[N_2–\mu–N_2]^+$ complex. The ZPE in the approximation schemes is shown in Figs. 10(a) and 10(b). The muon wavefunction is estimated to be significant on the length scale of the underlying crystal, making the quantum calculation necessary. Unfortunately, the two single-particle schemes give rather different

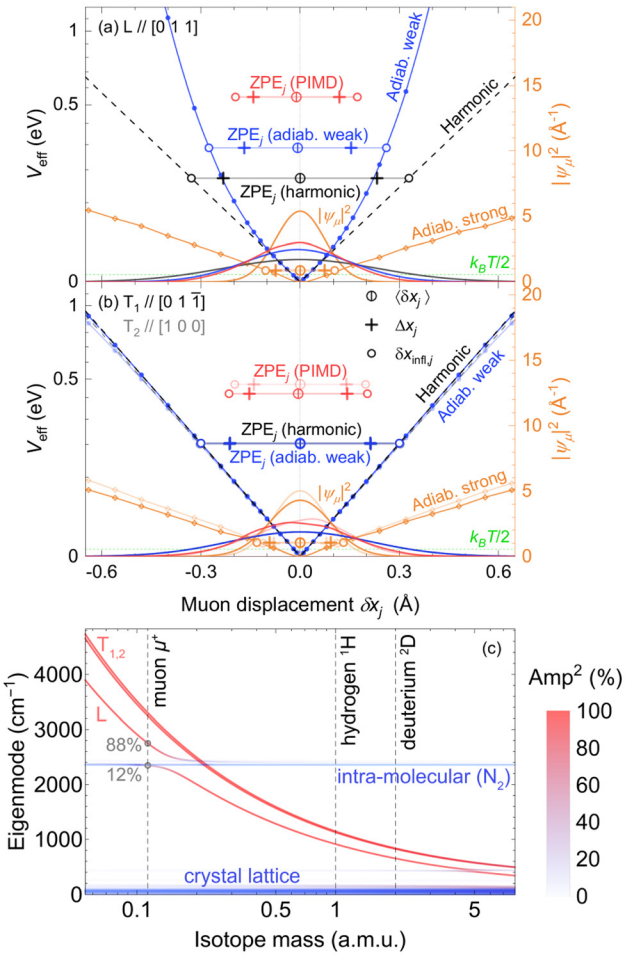

FIG. 10. (a) and (b) Effective muon potential in α–N_2 on a square-root linear scale (i.e., harmonic potentials appear as straight lines) along different directions for different approximations (left axis) with the corresponding muon probability density (right axis), directional contributions, mean muon displacements, wavefunction widths and inflection points. (c) Γ-point phonon spectra for muonated α-N_2 vs muon mass. Shading gives the muon amplitude squared in the normal modes. Reproducedwith permission from Gomilšek *et al.*, "Many-body quantum muon effects and quadrupolar coupling in solid nitrogen," arXiv:2202.05859 (2022).[87]

estimates of the ZPE. The phonon calculation [shown in Fig. 10(c) as a function of muon mass] shows the problem here: a strong hybridization of the longitudinal muon normal mode with intra-molecular vibrations of both N_2 in the $[N_2–\mu–N_2]^+$ complex, which implies significant muon-nuclear entanglement. As a result, both the single particle and harmonic approximations provide only a very rough guide to the quantum effects and do not agree between themselves. In cases such as that of N_2, an exact approach is, therefore, needed. This is carried out using path-integral molecular dynamics (PIMD), in which observables are calculated from arbitrary muon-nuclear zero-point motion. This scheme, based on discretizing an imaginary-time path integral, is very intensive on computer power, but can yield reliable numerical estimates. In the case of N_2, it confirms that the muon and

its surroundings are strongly entangled, but leads to a very precise estimate of the ^{14}N nuclear quadrupolar coupling constant.[87]

Continuing the theme of quantum mechanical effects, transition-state searches provide a route to evaluating the possibility of muon diffusion between candidate sites (an early example of this was applied to the study of muon diffusion in copper[61]). In a general geometry optimization process, the coordinates of the atoms are adjusted so that the energy of the structure is brought to a stationary point, in which the forces on the atoms are small. A transition state (TS) is a stationary point that is an energy maximum in one direction and an energy minimum in all other directions. A procedure that automates a search for TSs in codes such as CASTEP[38] is particularly useful for predicting barriers to chemical reactions and determining reaction pathways. In a chemical reaction, for example, starting from reactants, energy increases to a maximum and then decreases to the energy of the products. The maximum energy along the reaction pathway is the activation energy and the structure corresponding to this energy is the transition state. These ideas can be used to find diffusion barriers, which is where its use in μSR arises.

A recent example of the use of transition-state analysis to evaluate muon diffusion in a solid is the case of TaS_2.[88] Here, the muon sites form four distinct groups (Fig. 11). Muons in site 1 bond to one S atom in each of two adjacent TaS_2 layers forming a linear S–μ–S state with unequal bond lengths. In site 2, the muon is bonded to only a single S atom (with a bond length of 1.4 Å), with these sites being around 0.03 eV higher in energy than site 1. In site 3, the muon stops inside the S layer, slightly displaced from the center of the triangle defined by three S atoms. For site 4, the muon site is displaced by around 0.7 Å along the c-axis above the center of the triangle defined by three Ta atoms. To investigate the possibility of muon diffusion, TS searches between each pair of distinct muon stopping sites associated with a single TaS_2 layer were carried out. The energy barrier between sites 1 and 2 is very close to the difference in energy between the two. This, coupled with the large estimated ZPEs of both sites (0.35 and 0.51 eV, respectively), means that the muon is likely to be delocalized between these two geometries, rather than there being two distinct stopping sites. Similarly, the barrier between sites 2 and 3 is less than their ZPE. Thus, sites 1, 2, and 3 are expected to form a single quantum delocalized state.

V. OUTLOOK AND CONCLUSION

DFT + μ is computationally costly, particularly for complex materials, and each new material investigated has to be studied from scratch in the same way. Many of the most exciting materials that are currently being discovered (including spin liquids) tend to be chemically complex, and this puts severe demands on the feasibility of electronic structure calculations. Although we have concentrated on calculations of the muon site and associated local distortions, DFT calculations can also be used to estimate muon contact hyperfine fields in metals.[89,90]

The μSR technique concentrates on using the positive muon, but experiments with negative muons can also be performed.[4] There is no problem with identifying the μ^- site because it is captured by the nucleus. This does result in an atom with atomic number Z behaving as a muonic atom with effective nuclear charge $+(Z-1)e$, the μ^- partially screening the full nuclear charge. The effect on this state on the local crystal structure can then be calculated using DFT.[91] (This method can be termed DFT $+\mu^-$ to distinguish it from the usual DFT $+\mu^+$ technique.)

A notable feature of the method used in (positive muon) DFT $+\mu$ of randomly initializing muons in sites and then relaxing the structure is that it is rather unlike the real-life situation of the muon finding its stopping site by impinging on the sample with an energy of 4 MeV and then shedding energy through interactions with the solid, before eventually coming to rest.[4] This means that it is not possible, given an energy-ordered list of calculated muon sites, to tell which is realized, nor to reliably estimate the relative occupancy of several multiply occupied sites.

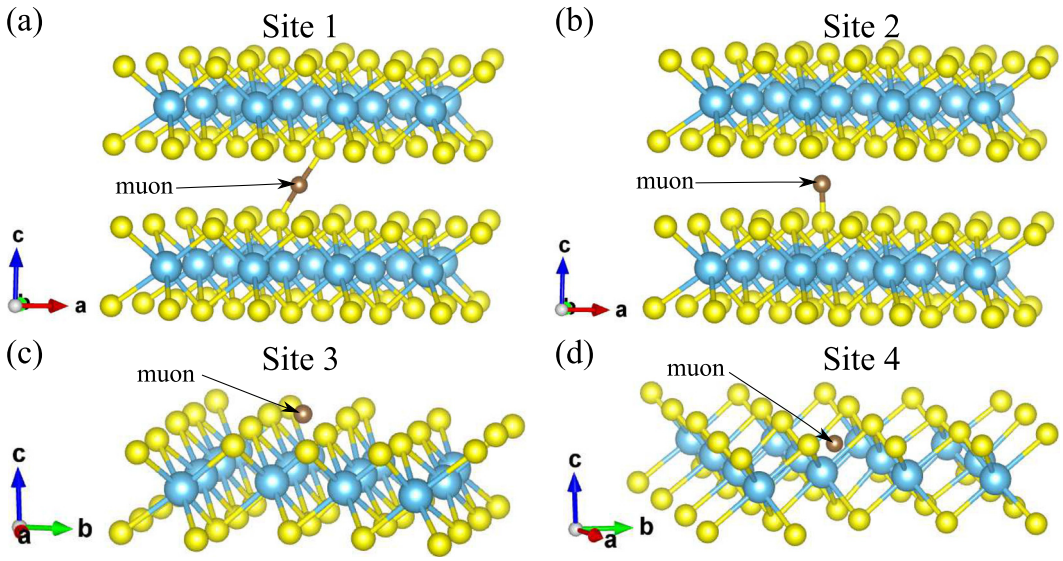

FIG. 11. Muon stopping sites in TaS_2. Ta and S are represented by blue and yellow spheres respectively. Sites 1 and 2 occupy the interlayer region. Site 3 is associated with the S layer and site 4 with the Ta layer. Reproduced with permission from Mañas-Valero *et al.*, npj Quantum Mater. **6**, 69 (2021). Copyright 2021 Springer Nature.[88]

Ultimately, a capture cross section for each site is needed, whose value will reflect not only the energy, but also some details of the final stages of the muon stopping process. This is likely to be an avenue of future research whose solution will allow further information to be squeezed from results obtained using the μSR technique. Nevertheless, the progress obtained within the last few years using DFT+μ has already transformed the way in which muon data are both interpreted and understood. Though this method is in its infancy, it has become an indispensable part of how muon experiments are now conducted.

ACKNOWLEDGMENTS

We are grateful to the following students, postdocs, and colleagues, who have collaborated with us in our research in this area and made important contributions to this field: Pietro Bonfà, Davide Ceresoli, Stewart Clark, Roberto De Renzi, Marina Filip, Francesca Foronda, George Gill, Matjaž Gomilšek, Zachary Hawkhead, Alberto Hernandez Melían, Thomas Hicken, Benjamin Huddart, Dominik Jochym, Mohammad Maikudi Isah, Franziska Kirschner, Franz Lang, Leandro Liborio, Nicola Marzari, Johannes Möller, Ifeanyi John Onuorah, Francis Pratt, Samuele Sanna, Simone Sturniolo, Johnny Wilkinson, and Hank Wu. We acknowledge funding from EPSRC(UK). S.J.B. acknowledges funding from UK Research and Innovation (UKRI) under the UK government's Horizon Europe funding guarantee (Grant No. EP/X025861/1).

AUTHOR DECLARATIONS

Conflict of Interest

The authors have no conflicts to disclose.

Author Contributions

Stephen J. Blundell: Writing – original draft (equal); Writing – review & editing (equal). **Tom Lancaster:** Writing – original draft (equal); Writing – review & editing (equal).

DATA AVAILABILITY

Data sharing is not applicable to this article as no new data were created or analyzed in this study.

REFERENCES

[1]S. F. J. Cox, "Implanted muon studies in condensed matter science," J. Phys. C **20**, 3187–3319 (1987).
[2]P. D. de Réotier and A. Yaouanc, "Muon spin rotation and relaxation in magnetic materials," J. Phys.: Condens. Matter **9**, 9113–9166 (1997).
[3]S. J. Blundell, "Spin-polarized muons in condensed matter physics," Contemp. Phys. **40**, 175–192 (1999).
[4]*Muon Spectroscopy—An Introduction*, edited by S. J. Blundell, R. D. Renzi, T. Lancaster, and F. L. Pratt (Oxford University Press, Oxford, 2022).
[5]R. L. Garwin, L. M. Lederman, and M. Weinrich, "Observations of the failure of conservation of parity and charge conjugation in meson decays: The magnetic moment of the free muon," Phys. Rev. **105**, 1415–1417 (1957).
[6]C. V. Topping and S. J. Blundell, "AC susceptibility as a probe of low-frequency magnetic dynamics," J. Phys.: Condens. Matter **31**, 013001 (2019).
[7]A. T. Boothroyd, *Principles of Neutron Scattering From Condensed Matter* (Oxford University Press, Oxford, 2019).
[8]J. E. Sonier, J. H. Brewer, and R. F. Kiefl, "μSR studies of the vortex state in type-II superconductors," Rev. Mod. Phys. **72**, 769–811 (2000).
[9]S. J. Blundell, "Muon-spin rotation studies of electronic properties of molecular conductors and superconductors," Chem. Rev. **104**, 5717–5735 (2004).
[10]J. S. Möller, D. Ceresoli, T. Lancaster, N. Marzari, and S. J. Blundell, "Quantum states of muons in fluorides," Phys. Rev. B **87**, 121108 (2013).
[11]F. Bernardini, P. Bonfà, S. Massidda, and R. De Renzi, "*Ab initio* strategy for muon site assignment in wide band gap fluorides," Phys. Rev. B **87**, 115148 (2013).
[12]J. S. Möller, P. Bonfà, D. Ceresoli, F. Bernardini, S. J. Blundell, T. Lancaster, R. D. Renzi, N. Marzari, I. Watanabe, S. Sulaiman, and M. I. Mohamed-Ibrahim, "Playing quantum hide-and-seek with the muon: Localizing muon stopping sites," Phys. Scr. **88**, 068510 (2013).
[13]P. Bonfà and R. De Renzi, "Toward the computational prediction of muon sites and interaction parameters," J. Phys. Soc. Jpn. **85**, 091014 (2016).
[14]W. Kohn, "Nobel Lecture: Electronic structure of matter—wave functions and density functionals," Rev. Mod. Phys. **71**, 1253–1266 (1999).
[15]J. H. Brewer, R. F. Kiefl, J. F. Carolan, P. Dosanjh, W. N. Hardy, S. R. Kreitzman, Q. Li, T. M. Riseman, P. Schleger, H. Zhou, E. J. Ansaldo, D. R. Noakes, L. P. Le, G. Luke, Y. J. Uemura, K. Hepburn-Wiley, and C. E. Stronach, "Site of the positive muon in $YBa_2Cu_3O_7$," Hyp. Int. **63**, 177–182 (1990).
[16]J. Demaison, M. Herman, and J. Lievin, "The equilibrium OH bond length," Int. Rev. Phys. Chem. **26**, 391–420 (2007).
[17]J. H. Brewer, S. R. Kreitzman, D. R. Noakes, E. J. Ansaldo, D. R. Harshman, and R. Keitel, "Observation of muon-fluorine 'hydrogen bonding' in ionic crystals," Phys. Rev. B **33**, 7813–7816 (1986).
[18]G. M. Luke, J. H. Brewer, S. R. Kreitzman, D. R. Noakes, M. Celio, R. Kadono, and E. J. Ansaldo, "Muon diffusion and spin dynamics in copper," Phys. Rev. B **43**, 3284–3297 (1991).
[19]S. J. Blundell, A. J. Steele, T. Lancaster, J. D. Wright, and F. L. Pratt, "A Bayesian approach to magnetic moment determination using μSR," Phys. Procedia **30**, 113–116 (2012).
[20]A. J. Steele, P. J. Baker, T. Lancaster, F. L. Pratt, I. Franke, S. Ghannadzadeh, P. A. Goddard, W. Hayes, D. Prabhakaran, and S. J. Blundell, "Low-moment magnetism in the double perovskites Ba_2MOsO_6 (M = Li, Na)," Phys. Rev. B **84**, 144416 (2011).
[21]S. M. Disseler, "Direct evidence for the all-in/all-out magnetic structure in the pyrochlore iridates from muon spin relaxation," Phys. Rev. B **89**, 140413 (2014).
[22]G. Prando, P. Telang, S. D. Wilson, M. J. Graf, and S. Singh, "Monopole-limited nucleation of magnetism in $Eu_2Ir_2O_7$," Phys. Rev. B **101**, 174435 (2020).
[23]J. H. Van Vleck, "The dipolar broadening of magnetic resonance lines in crystals," Phys. Rev. **74**, 1168–1183 (1948).
[24]A. Abragam, *Principles of Nuclear Magnetism* (Oxford University Press, Oxford, 1961).
[25]C. P. Slichter, *Principles of Magnetic Resonance*, 3rd ed. (Springer, Berlin, 1990).
[26]F. Giustino, *Materials Modelling Using Density Functional Theory: Properties and Predictions* (Oxford University Press, Oxford, 2014).
[27]P. Hohenberg and W. Kohn, "Inhomogeneous electron gas," Phys. Rev. **136**, B864–B871 (1964).
[28]W. Kohn and L. J. Sham, "Self-consistent equations including exchange and correlation effects," Phys. Rev. **140**, A1133–A1138 (1965).
[29]A. D. Becke, "Density-functional thermochemistry. III. The role of exact exchange," J. Chem. Phys **98**, 5648–5652 (1993).
[30]J. P. Perdew, K. Burke, and M. Ernzerhof, "Generalized gradient approximation made simple," Phys. Rev. Lett. **77**, 3865–3868 (1996).
[31]K. Burke, "Perspective on density functional theory," J. Chem. Phys. **136**, 150901 (2012).
[32]C. Freysoldt, B. Grabowski, T. Hickel, J. Neugebauer, G. Kresse, A. Janotti, and C. G. Van de Walle, "First-principles calculations for point defects in solids," Rev. Mod. Phys. **86**, 253–305 (2014).
[33]M. Leslie and N. J. Gillan, "The energy and elastic dipole tensor of defects in ionic crystals calculated by the supercell method," J. Phys. C **18**, 973 (1985).
[34]G. Makov and M. C. Payne, "Periodic boundary conditions in *ab initio* calculations," Phys. Rev. B **51**, 4014–4022 (1995).
[35]C. G. Van de Walle, "Energies of various configurations of hydrogen in silicon," Phys. Rev. B **49**, 4579–4585 (1994).

[36]P. Giannozzi, S. Baroni, N. Bonini, M. Calandra, R. Car, C. Cavazzoni, D. Ceresoli, G. L. Chiarotti, M. Cococcioni, I. Dabo, A. D. Corso, S. de Gironcoli, S. Fabris, G. Fratesi, R. Gebauer, U. Gerstmann, C. Gougoussis, A. Kokalj, M. Lazzeri, L. Martin-Samos, N. Marzari, F. Mauri, R. Mazzarello, S. Paolini, A. Pasquarello, L. Paulatto, C. Sbraccia, S. Scandolo, G. Sclauzero, A. P. Seitsonen, A. Smogunov, P. Umari, and R. M. Wentzcovitch, "QUANTUM ESPRESSO: A modular and open-source software project for quantum simulations of materials," J. Phys.: Condens. Matter **21**, 395502 (2009).
[37]B. Huddart, A. Hernández-Melián, T. Hicken, M. Gomilšek, Z. Hawkhead, S. Clark, F. Pratt, and T. Lancaster, "MuFinder: A program to determine and analyse muon stopping sites," Comput. Phys. Commun. **280**, 108488 (2022).
[38]S. J. Clark, M. D. Segall, C. J. Pickard, P. J. Hasnip, M. I. J. Probert, K. Refson, and M. C. Payne, "First principles methods using CASTEP," Z. Kristallogr.-Cryst. Mater. **220**, 567–570 (2005).
[39]P. Bonfà, I. J. Onuorah, and R. D. Renzi, "Introduction and a quick look at muesr, the magnetic structure and muon embedding site refinement suite," JPS Conf. Proc. **21**, 011052 (2018).
[40]L. Liborio, S. Sturniolo, and D. Jochym, "Computational prediction of muon stopping sites using ab initio random structure searching (AIRSS)," J. Chem. Phys. **148**, 134114 (2018).
[41]C. J. Pickard and R. J. Needs, "*Ab initio* random structure searching," J. Phys.: Condens. Matter **23**, 053201 (2011).
[42]S. Sturniolo and L. Liborio, "Computational prediction of muon stopping sites: A novel take on the unperturbed electrostatic potential method," J. Chem. Phys. **153**, 044111 (2020).
[43]T. Lancaster and S. Blundell, *Quantum Field Theory for the Gifted Amateur* (Oxford University Press, Oxford, 2014).
[44]S. Sturniolo, L. Liborio, and S. Jackson, "Comparison between density functional theory and density functional tight binding approaches for finding the muon stopping site in organic molecular crystals," J. Chem. Phys. **150**, 154301 (2019).
[45]J. M. Ziman, *Principles of the Theory of Solids*, 2nd ed. (Cambridge University Press, Cambridge, 1972).
[46]D. R. Noakes, E. J. Ansaldo, S. R. Kreitzman, and G. M. Luke, "The $(F\mu F)^-$ ion in solid fluorides," J. Phys. Chem. Solids **54**, 785 (1993).
[47]F. L. Pratt, S. J. Blundell, I. M. Marshall, T. Lancaster, A. Husmann, C. Steer, W. Hayes, C. Fischmeister, R. E. Martin, and A. B. Holmes, "μSR in polymers," Physica B **326**, 34 (2003).
[48]K. Nishiyama, S. Nishiyama, and W. Higemoto, "Asymmetric F–μ–F interaction of the muon in polyfluorocarbons," Physica B **326**, 41 (2003).
[49]T. Lancaster, F. L. Pratt, S. J. Blundell, I. McKenzie, and H. E. Assender, "Muon-fluorine entanglement in fluoropolymers," J. Phys.: Condens. Matter **21**, 346004 (2009).
[50]T. Lancaster, S. J. Blundell, P. J. Baker, M. L. Brooks, W. Hayes, F. L. Pratt, J. L. Manson, M. M. Conner, and J. A. Schlueter, "Muon-fluorine entangled states in molecular magnets," Phys. Rev. Lett. **99**, 267601 (2007).
[51]K. Kawaguchi and E. Hirota, "Diode laser spectroscopy of the ν_3 and ν_2 bands of FHF^{-1} in 1300 cm^{-1} region," J. Chem. Phys. **87**, 6838–6841 (1987).
[52]J. M. Wilkinson and S. J. Blundell, "Information and decoherence in a muon-fluorine coupled system," Phys. Rev. Lett. **125**, 087201 (2020).
[53]J. M. Wilkinson, F. L. Pratt, T. Lancaster, P. J. Baker, and S. J. Blundell, "Muon sites in PbF_2 and YF_3: Decohering environments and the role of anion Frenkel defects," Phys. Rev. B **104**, L220409 (2021).
[54]P. Bonfà, M. M. Isah, B. A. Frandsen, E. J. Gibson, E. Brück, I. J. Onuorah, R. De Renzi, and G. Allodi, "*Ab initio* modeling and experimental investigation of Fe_2P by DFT and spin spectroscopies," Phys. Rev. Mater. **5**, 044411 (2021).
[55]R. C. Williams, F. Xiao, I. O. Thomas, S. J. Clark, T. Lancaster, G. A. Cornish, S. J. Blundell, W. Hayes, A. K. Paul, C. Felser, and M. Jansen, "Muon-spin relaxation study of the double perovskite insulators Sr_2BOsO_6 (B=Fe, Y, In)," J. Phys.: Condens. Matter **28**, 076001 (2016).
[56]F. Lang, P. J. Baker, A. A. Haghighirad, Y. Li, D. Prabhakaran, R. Valentí, and S. J. Blundell, "Unconventional magnetism on a honeycomb lattice in α-$RuCl_3$ studied by muon spin rotation," Phys. Rev. B **94**, 020407 (2016).
[57]F. K. K. Kirschner, R. D. Johnson, F. Lang, D. D. Khalyavin, P. Manuel, T. Lancaster, D. Prabhakaran, and S. J. Blundell, "Spin Jahn-Teller antiferromagnetism in $CoTi_2O_5$," Phys. Rev. B **99**, 064403 (2019).
[58]F. Lang, L. Jowitt, D. Prabhakaran, R. D. Johnson, and S. J. Blundell, "$FeTi_2O_5$: A spin Jahn-Teller transition enhanced by cation substitution," Phys. Rev. B **100**, 094401 (2019).
[59]J. Sugiyama, K. Miwa, H. Nozaki, Y. Kaneko, B. Hitti, D. Arseneau, G. D. Morris, E. J. Ansaldo, and J. H. Brewer, "Magnetic moment of rare-earth elements in $R_2Fe_{14}B$ estimated with μ^+SR," Phys. Rev. Mater. **3**, 064402 (2019).
[60]A. Amato, P. Dalmas de Réotier, D. Andreica, A. Yaouanc, A. Suter, G. Lapertot, I. M. Pop, E. Morenzoni, P. Bonfà, F. Bernardini, and R. De Renzi, "Understanding the μSR spectra of MnSi without magnetic polarons," Phys. Rev. B **89**, 184425 (2014).
[61]P. Bonfá, F. Sartori, and R. De Renzi, "Efficient and reliable strategy for identifying muon sites based on the double adiabatic approximation," J. Phys. Chem. C **119**, 4278–4285 (2015).
[62]V. G. Storchak, J. H. Brewer, R. L. Lichti, T. A. Lograsso, and D. L. Schlagel, "Electron localization into spin-polaron state in MnSi," Phys. Rev. B **83**, 140404 (2011).
[63]K. J. A. Franke, B. M. Huddart, T. J. Hicken, F. Xiao, S. J. Blundell, F. L. Pratt, M. Crisanti, J. A. T. Barker, S. J. Clark, A. Štefančič, M. C. Hatnean, G. Balakrishnan, and T. Lancaster, "Magnetic phases of skyrmion-hosting $GaV_4S_{8-y}Se_y$ ($y = 0, 2, 4, 8$) probed with muon spectroscopy," Phys. Rev. B **98**, 054428 (2018).
[64]T. Lancaster, "Skyrmions in magnetic materials," Contemp. Phys. **60**, 246–261 (2019).
[65]K. Tustain, B. Ward-O'Brien, F. Bert, T. Han, H. Luetkens, T. Lancaster, B. M. Huddart, P. J. Baker, and L. Clark, "From magnetic order to quantum disorder in the Zn-barlowite series of S = 1/2 kagomé antiferromagnets," npj Quantum Mater. **5**, 74 (2020).
[66]C. G. Van de Walle, "Hydrogen as a cause of doping in zinc oxide," Phys. Rev. Lett. **85**, 1012–1015 (2000).
[67]S. F. J. Cox, "Muonium as a model for interstitial hydrogen in the semiconducting and semimetallic elements," Rep. Prog. Phys. **72**, 116501 (2009).
[68]M. Hiraishi, H. Okabe, A. Koda, R. Kadono, and H. Hosono, "Ambipolarity of diluted hydrogen in wide-gap oxides revealed by muon study," J. Appl. Phys. **132**, 105701 (2022).
[69]M. H. Dehn, J. K. Shenton, S. Holenstein, Q. N. Meier, D. J. Arseneau, D. L. Cortie, B. Hitti, A. C. Y. Fang, W. A. MacFarlane, R. M. L. McFadden, G. D. Morris, Z. Salman, H. Luetkens, N. A. Spaldin, M. Fechner, and R. F. Kiefl, "Observation of a charge-neutral muon-polaron complex in antiferromagnetic Cr_2O_3," Phys. Rev. X **10**, 011036 (2020).
[70]M. H. Dehn, J. K. Shenton, D. J. Arseneau, W. A. MacFarlane, G. D. Morris, A. Maigné, N. A. Spaldin, and R. F. Kiefl, "Local electronic structure and dynamics of muon-polaron complexes in Fe_2O_3," Phys. Rev. Lett. **126**, 037202 (2021).
[71]M. R. Ramadhan, B. Adiperdana, I. Ramli, D. P. Sari, A. E. Putri, U. Widyaiswari, H. b. Rozak, W. N. Zaharim, A. Manaf, B. Kurniawan, M. I. Mohamed-Ibrahim, S. Sulaiman, T. Kawamata, T. Adachi, Y. Koike, and I. Watanabe, "Estimation of the on-site Coulomb potential and covalent state in La_2CuO_4 by muon spin rotation and density functional theory calculations," Phys. Rev. Res. **4**, 033044 (2022).
[72]R. De Renzi, P. Bonfà, M. Mazzani, S. Sanna, G. Prando, P. Carretta, R. Khasanov, A. Amato, H. Luetkens, M. Bendele, F. Bernardini, S. Massidda, A. Palenzona, M. Tropeano, and M. Vignolo, "Effect of external pressure on the magnetic properties of LnFeAsO (Ln = La, Ce, Pr, Sm)," Supercond. Sci. Technol. **25**, 084009 (2012).
[73]S. C. Cheung, Z. Guguchia, B. A. Frandsen, Z. Gong, K. Yamakawa, D. E. Almeida, I. J. Onuorah, P. Bonfá, E. Miranda, W. Wang, D. W. Tam, Y. Song, C. Cao, Y. Cai, A. M. Hallas, M. N. Wilson, T. J. S. Munsie, G. Luke, B. Chen, G. Dai, C. Jin, S. Guo, F. Ning, R. M. Fernandes, R. De Renzi, P. Dai, and Y. J. Uemura, "Disentangling superconducting and magnetic orders in $NaFe_{1-x}Ni_xAs$ using muon spin rotation," Phys. Rev. B **97**, 224508 (2018).
[74]S. Sundar, N. Azari, M. R. Goeks, S. Gheidi, M. Abedi, M. Yakovlev, S. R. Dunsiger, J. M. Wilkinson, S. J. Blundell, T. E. Metz, I. M. Hayes, S. R. Saha, S. Lee, A. J. Woods, R. Movshovich, S. M. Thomas, N. P. Butch, P. F. S. Rosa, J. Paglione, and J. E. Sonier, "Ubiquitous spin freezing in the superconducting state of UTe_2," Commun. Phys. **6**, 24 (2023).
[75]B. M. Huddart, I. J. Onuorah, M. M. Isah, P. Bonfà, S. J. Blundell, S. J. Clark, R. De Renzi, and T. Lancaster, "Intrinsic nature of spontaneous magnetic fields in

superconductors with time-reversal symmetry breaking," Phys. Rev. Lett. **127**, 237002 (2021).
[76]B. M. Huddart, M. Gomilšek, T. J. Hicken, F. L. Pratt, S. J. Blundell, P. A. Goddard, S. J. Kaech, J. L. Manson, and T. Lancaster, "Magnetic order and ballistic spin transport in a sine-Gordon spin chain," Phys. Rev. B **103**, L060405 (2021).
[77]S. Eggert and I. Affleck, "Magnetic impurities in half-integer-spin Heisenberg antiferromagnetic chains," Phys. Rev. B **46**, 10866–10883 (1992).
[78]J. A. Chakhalian, R. F. Kiefl, R. Miller, J. Brewer, S. R. Dunsiger, G. Morris, W. A. MacFarlane, J. E. Sonier, S. Eggert, I. Affleck, A. Keren, and M. Verdaguer, "Local magnetic susceptibility of the positive muon in the quasi-one-dimensional $S = 1/2$ antiferromagnet dichlorobis (pyridine) copper (II)," Phys. Rev. Lett. **91**, 027202 (2003).
[79]F. Xiao, J. S. Möller, T. Lancaster, R. C. Williams, F. L. Pratt, S. J. Blundell, D. Ceresoli, A. M. Barton, and J. L. Manson, "Spin diffusion in the low-dimensional molecular quantum Heisenberg antiferromagnet $Cu(pyz)(NO_3)_2$ detected with implanted muons," Phys. Rev. B **91**, 144417 (2015).
[80]T. Lancaster, F. Xiao, B. M. Huddart, R. C. Williams, F. L. Pratt, S. J. Blundell, S. J. Clark, R. Scheuermann, T. Goko, S. Ward, J. L. Manson, C. Rüegg, and K. W. Krämer, "Quantum magnetism in molecular spin ladders probed with muon-spin spectroscopy," New J. Phys. **20**, 103002 (2018).
[81]S. J. Blundell, J. S. Möller, T. Lancaster, P. J. Baker, F. L. Pratt, G. Seber, and P. M. Lahti, "μSR study of magnetic order in the organic quasi-one-dimensional ferromagnet F4BImNN," Phys. Rev. B **88**, 064423 (2013).
[82]F. R. Foronda, F. Lang, J. S. Möller, T. Lancaster, A. T. Boothroyd, F. L. Pratt, S. R. Giblin, D. Prabhakaran, and S. J. Blundell, "Anisotropic local modification of crystal field levels in Pr-based pyrochlores: A muon-induced effect modeled using density functional theory," Phys. Rev. Lett. **114**, 017602 (2015).
[83]H. D. Zhou, C. R. Wiebe, J. A. Janik, L. Balicas, Y. J. Yo, Y. Qiu, J. R. D. Copley, and J. S. Gardner, "Dynamic spin ice: $Pr_2Sn_2O_7$," Phys. Rev. Lett. **101**, 227204 (2008).
[84]A. J. Princep, D. Prabhakaran, A. T. Boothroyd, and D. T. Adroja, "Crystal-field states of Pr^{3+} in the candidate quantum spin ice $Pr_2Sn_2O_7$," Phys. Rev. B **88**, 104421 (2013).
[85]B. Bleaney, "Enhanced nuclear magnetism," Physica **69**, 317–329 (1973).
[86]S. J. Blundell, "The quantum muon," J. Phys.: Conf. Ser. **2462**, 012001 (2023).
[87]M. Gomilšek, F. L. Pratt, S. P. Cottrell, S. J. Clark, and T. Lancaster, "Many-body quantum muon effects and quadrupolar coupling in solid nitrogen," arXiv:2202.05859 (2022).
[88]S. Mañas-Valero, B. M. Huddart, T. Lancaster, E. Coronado, and F. L. Pratt, "Quantum phases and spin liquid properties of 1T-TaS_2," npj Quantum Mater. **6**, 69 (2021).
[89]I. J. Onuorah, P. Bonfà, and R. De Renzi, "Muon contact hyperfine field in metals: A DFT calculation," Phys. Rev. B **97**, 174414 (2018).
[90]I. J. Onuorah, P. Bonfà, R. De Renzi, L. Monacelli, F. Mauri, M. Calandra, and I. Errea, "Quantum effects in muon spin spectroscopy within the stochastic self-consistent harmonic approximation," Phys. Rev. Mater. **3**, 073804 (2019).
[91]G. J. W. Gill, F. L. Pratt, and S. J. Blundell, "Extending WiMDA for the data analysis of μ^- SR experiments," J. Phys.: Conf. Ser. **2462**, 012010 (2023).